Aalto-yliopisto
Aalto-universitetet
Aalto University

Master's Programme in Mechanical Engineering

Comparative life cycle inventory of CNC machining and powder bed fusion additive manufacturing

Comparative assessment of the materials and energy flow for three metal components manufactured by CNC machining and powder bed fusion

Juan Silva

Master's Thesis
2022

Author Juan Silva

Title of thesis Comparative life cycle inventory of CNC machining and powder bed fusion Additive Manufacturing

Programme Mechanical Engineering

Major Product Development

Thesis supervisor Prof. Kalevi Ekman

Thesis advisor Joni Reijonen, MSc. VTT Oy.

Collaborative partner Thesis for VTT, Technical Research Centre of Finland Ltd.

Date 29.12.2022 **Number of pages** 88 **Language** English

Abstract

This thesis work aims to produce a life cycle inventory (LCI) in the comparison between one method from advanced manufacturing (AM) and one method from conventional manufacturing (CM). For the AM, a powder bed fusion laser beam (PBF-LB) has been utilized, and for CM, CNC-mill and CNC-lathe has been utilized. The comparative assessment was performed for the manufacturing phase of three different metal components. Two of the components are commercial products from SEW-Eurodrive Oy and Proventia Oy. The third component is a spur gear optimized and designed by the author for AM and a solid gear for CNC-machining. Most of the components were manufactured from stainless steel 316L, but the SEW component manufactured with CNC was made of 11SMn30+C. The three components have been 3D printed with an SLM 125 HL. For post-processing, EDM was utilized to separate the build plates and CNC for the final operations. Similarly, the three components were manufactured with a CNC mill, and the SEW part was also made with a CNC lathe. The experiments performed in this thesis aim to replicate a real-life manufacturing scenario while measuring the input values. Hence, efforts have been made to reproduce the functional characteristic of the components, such as tolerances, thread sizes and surface roughness. These experiments aimed for accurate measurements of the consumables, such as argon gas and raw material waste. Energy meter devices were installed in all the machines to obtain electricity consumption during the operations and stand-by procedures. The results for the energy consumption were higher for the PBF than the CNC machining in all the components. The Proventia and SEW components manufactured with CNC-mill had higher material waste than those manufactured with PBF. The finished part weight from the optimized gear manufactured in PBF was 40% lighter than the solid gear manufactured with CNC-mill. The waste for the optimized gear manufactured with PBF was 69% greater than the solid gear made with CNC-mill. Both required almost the same total raw material input. The Proventia part was manufactured twice in PBF with a 30 µm and 50 µm layer thickness. The 50 µm layer thickness component consumed 10% less energy and argon gas and generated 16% less waste. The SLM 125 HL consumed 1.145 kg of argon gas to fill the chamber before printing. This SLM machine has a single laser and consumed an average of 2.3 kWh during the utilization of the laser and 1.35 kWh when the laser was not melting. The material waste of the filters and sieving from the SLM process were higher than expected.

Keywords Life Cycle inventory, Additive Manufacturing, Powder bed fusion laser beam, CNC-machining.

Contents

Figures

Tables

Preface

This thesis was performed for Aalto University under Mechanical Engineering master program department. The responsible company was VTT, Technical Research Centre of Finland Ltd., which provided this thesis topic for one of their projects.

I want to show gratitude to Professor Kalevi Ekman, Supervisor of the thesis, for all your help and guidance during my studies at Aalto University Design Factory. You have been of great assistance, and thanks to You, I have made many new friends and helped me to find work in Finland at VTT.

From the side of VTT, I want to express my gratitude to the thesis instructor Joni Reijonen, MSc. You have given me your time and energy since the start of the thesis. Your great research scientist skills have helped me to accomplish this scientific report. Special thanks to Kimmo Ruusuvuori, research Engineer at VTT's AM lab, that has always been open to kindly teaching me the processes in the laboratory. I want to fast my gratefulness to Pasi Puukko and Sini Metsä-Kortelainen for being generous and helpful as my supervisors during my thesis work at VTT.

Finally, I want to thank my family for being the support system and inspiration for my academic career in Finland, as well as all my friends for their encouragement and care as I wrote my thesis.

Otaniemi, 30 December 2022
Juan Silva

Abbreviations

AM	Additive manufacturing
CAD	Computer-aided design
CM	Conventional manufacturing
CNC	Control numeric computerised
DfAM	Design for additive manufacturing
EDM	Electrical discharge machine
LCA	Life cycle assessment
LCI	Life cycle inventory
PBF-LB	Powder bed fusion laser beam
PM	Powder metallurgic
PPM	Parts per million
SEC	Specific energy consumption
SLM	Selective laser melting
STL	Stereolithography

1 Introduction

1.1 Background

The industrial revolution has advanced exponentially faster in the last decades than in the previous century, and the carbon emissions released into the atmosphere have grown alarmingly. (World Economic Forum, 2016) From January 2022 until November 2022, the emissions released in the air were 36 billion tons of CO2 from all human activities, and it is expected that it will reach 43 billion tons of CO2 still this year. (Global Carbon Project, 2022) The temperature of the planet has also been rising dramatically along with the rest of the greenhouse gasses, and it is estimated that the temperature has increased by approximately 1.1 degrees Celsius since 1880. (NASA Earth Observatory, 2022) Since the 2015 Paris agreement, countries have committed to limit the increase of the planet's temperature by 1.5 degrees Celsius. (UNFCCC, 2015)

As part of the European Union, Finland has a common goal of carbon neutrality for the year 2050. Nevertheless, the goal of the Finnish government is substantially more forceful by setting the target for 2035 to become carbon neutral. (Finland Ministry of Environment, 2022) Manufacturing is Finland's most significant industry, making up over 87 per cent of all production. (Trading Economics, 2022) In other words, with an 87% share, manufacturing is the most important activity under the "Industrial production" business category. As a result, manufacturing in the industrial production segment accounts for 21.75% of the total Finnish GDP. (Statista, 2022) The direct emissions from energy usage are 6,079 M tones of CO2 equivalent released from manufacturing industries and construction in the year 2020 in Finland alone. (European Environment Agency, 2022) The Finnish manufacturing industry follows the low-carbon road map plan to reduce emissions that utilize electrification processes and machines, improve energy and material efficiency, and implement a circular economy with digital solutions. (Teknologiateollisuus, 2020) Due to such factors, Finland is investing in research for carbon-neutral solutions and sustainable materials, creating new technologies to mitigate climate change for future generations to have carbon-neutral manufacturing. (Toolbox Finland, 2021)

Some of the technology utilized in Finland includes digital solutions, such as additive manufacturing (AM) with metal 3D printing, that could play an important role in fighting climate change. (Liao & Cooper, 2021) Numerous studies imply that AM utilizes a lower amount of material than conventional manufacturing (CM), and it is therefore recognized as a low-carbon manufacturing process. (Liu et al., 2018; Böc kin and Tillman, 2019; Deboer et al., 2021) Nevertheless, it must be taken into consideration that AM has a higher embodied specific energy than CM for the material feedstock because of the

metal powder manufacturing. (Fredriksson, 2019) Other studies suggest that AM will never substitute CM, and a deeper and more holistic approach should be applied to better understand AM's environmental impacts and benefits. (Peng et al., 2018) There is literature available that compares both types of manufacturing processes through a Life Cycle Inventory (LCI), where the energy and input values are measured. (Van Sice & Faludi, 2021) However, Ochs et al. (2021) make additional recommendations for a more specific experimental approach in the measurements of the energy consumption and the input values for the LCIs.

The definition of sustainability is the ability to maintain something over an extended period. It signifies that everything that is sustainable may be maintained. (Duque Ciceri, 2010) For all these reasons, there is a necessity to perform a life cycle inventory comparison between different manufacturing methods with reliable and accurate data. It is also essential to compare different types of geometries and functionalities.

This master's thesis is part of the Green Factory Design Tool Kit (GREEF), a project funded by Business Finland and co-created by VTT's Advanced Manufacturing Technologies team, and it aims for carbon-neutral production in Finland. There are six companies involved in this project, as well as Oulu University and Aalto University acting as the coordinator. (University of Oulu, 2022) For this thesis work, the companies providing the case components are SEW Eurodrive Oy and Proventia Oy to VTT. The overall objective is to collect input data and conduct experimental trials with these participating companies as well as a literature review related to material, energy flows and emissions. (Aalto University, 2022)

1.2 Aim of the thesis

This thesis aims to produce a life cycle inventory comparison from three metal components manufactured with powder bed fusion laser beam PBF-LB and CNC-machining. These experiments attempt to replicate a real-life manufacturing scenario while measuring the input values from the production phase of the parts. The objective is to generate reliable and accurate data from the use of raw materials, energy, and argon gas. This study will include a literature review from previous publications comparing both methods (AM & CM).

In addition, the comparative LCI from the case components produced at VTT will be compared with existing literature. The results of this thesis intend to be utilized as a tool for companies to support and achieve better decisions towards carbon-neutral manufacturing. The final goal is to provide the necessary information to produce a life cycle assessment (LCA) study of the commercial components later in the GREEF project.

Research questions

This dissertation seeks to respond to the following research questions:

- How much argon gas, metal powder and electricity are required to manufacture each component with PBF-LB?
- How much feedstock material and electricity are required to manufacture each component with CNC-machining?
- Which method is most suitable to manufacture with the least consumption of input materials?
- What are the most relevant inputs flows for LCI of these manufacturing methods?

1.3 Research strategy and scope

In order to achieve this project successfully within a time length satisfactory for a master thesis, the scope restricts the number of stages of this LCI. From the point of view of an LCI, the scope was to only measure the primary data of production of the components during the manufacturing stage. During all the experiments, the machine operators and the author aimed to perform a proper process in the manufacturing system selections. This aided in maintaining proximity to a real-life manufacturing scenario.

The case component given by Proventia Oy is an impeller, and the second component from SEW Eurodrive is a manifold. Both companies have provided VTT with CAD models and 2D drawings for manufacturing. The third component is a spur gear designed by the author in the 3D modelling software Solid-Works. For this LCI comparison, there are two different CAD files for the spur gears. One spur gear is optimized for AM by design with a lattice pattern for less material consumption and weight reduction. The second spur gear is solid to only be CNC-machined.

The three components were manufactured at VTT's Additive manufacturing laboratory in Espoo. Similarly, the three components were CNC-machined with lathe and milling machines at the Oulu University machine shop. The three 3D-printed components were sent to Oulu university for final machining to achieve surface roughness, make threads and remove supports from the parts. The material utilized for the manufacturing was two different types of steel.

The measurement of electricity was performed with an ABB energy meter installed in the SLM 125 HL. The same ABB energy meter was utilized for the energy measurement to separate the 3D-printed parts from the SLM-build plate. This operation was completed at the Aalto university machining shop with a wire-cutting machine, Charmilles Robofil 440. Oulu university utilized a Shelly EM energy meter installed in a CNC-lathe machine Okuma LB 3000 EX II, and in the CNC-milling machine, GF Mill E 700 U.

A literature survey on the LCA comparison between AM and CM methods is included in this study. The scientific data available were compared with the findings from this project and analysed. The thesis has been concluded with recommendations for further studies.

1.3.1 Limitations

The following list describes in detail what will not be included or is neglected in this LCI for the CNC-machining and the 3D printing:

1. Manufacturing phase of raw materials: argon gas, metals feedstocks and cooling or cutting fluid of the machines.
2. The manufacturing phase of the machines utilized.
3. Transport of materials or machines.
4. Powder sieving, drying, vacuum cleaning, or the energy consumption of other auxiliary equipment.
5. Tool wear from CNC-machining and parts worn-out or consumables from the machines.
6. Optimization of the CNC-machining process for lowering energy consumption and emissions.
7. Software topology optimization of the CAD parts for weight reduction
8. Measuring water and cutting fluid consumption.
9. Use-phase and end-of-life of the three components.

The following points from the above list have been neglected in this LCI due to the following reasons:

Point four

The powder was dried in the oven with a vacuum at 60 degrees Celsius for some of the prints only because there was powder available inside the SLM canister before starting some of the prints; hence this process was neglected. Some parts have been cleaned with the ultrasonic cleaner to remove any left-over powder from the part that could become hazardous for handling, but the measurement of the energy of this is also ignored. Finally, the SLM machine requires a vacuum cleaner to suck the powder out of the chamber every time a print has been finalized, but this process is not accounted for.

Point five

Several tools were utilized for the CNC-machining operations of the three components. The operating time of the individual tools was short. Different tools cause different emission values, and the tools should run for an extended period to obtain reliable and comparable results. The wire-cutting

machine consumes wire for cutting because the wire can break easily. After all, the build plate is slightly deformed after 3D printing. A wire cutting machine was used rather than a expand saw machine because it is more precise, with up to 0.1 mm cutting precision. The wire-cutting machine also produces less waste than the expanded saw. The SLM machine consumes powder filters and a rubber wiper for the re-coater mechanism, but those consumables are not always the same amount for all the prints and were neglected in this study.

Point seven

The author's gear optimization has been designed manually in the 3D CAD software with a lattice pattern around the gear, meaning without the topology optimization algorithms. A scientific article on weight reduction for a 3D-printed gear with a lattice structure has inspired the design. In order to avoid supports inside the gear, the author has chosen a similar pattern as the lattice inside the gear.

Point eight

The evaporation of the cooling fluid has been neglected because the lubricants circulate inside the machine, which is very difficult to estimate. Also, the cutting fluid consumption is mainly based on evaporation which happens all the time and outflow via exhaust air with the workpiece and cutting chips. Therefore, in order to be able to get fact-based information about this consumption, the measurement should be performed for a sufficiently long period (days/weeks) to calculate more precise values.

2 Literature review

2.1 Life cycle inventory

Currently, several factors are encouraging industrial companies to make more environmentally friendly decisions. The most powerful tool to estimate a process or environmental and resource consumption of a product is to perform a life cycle assessment. This type of assessment is divided into four stages: Principal and framework (ISO 14040), Goal and scope definition and inventory analysis (ISO 14041), Life cycle impact assessment (ISO 14042) and Life cycle interpretation (ISO 14043), as seen in figure 1 (ISO 14040:2006, 2006).

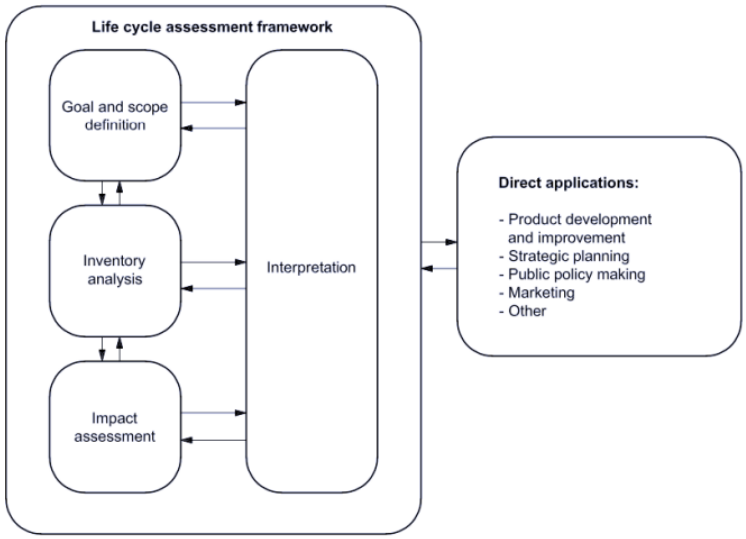

Figure 1, LCA framework (ISO 14040:2006, 2006).

Figure 1 shows the goal and scope from the framework of the LCA to be the first stage to be executed when following the standards. In this stage, the accuracy and depth of the LCA are decided together with all the stakeholders. (Grahl B &. Klöpffer, 2014) It is essential to notice that both the goal and scope can change prominently during the study due to the interactive nature of LCA. (ISO 14040:2006, 2006) The life cycle inventory can be started when the goal and scope are defined. According to ISO 14040:2006 (2006), "the inventory analysis is the phase of the LCA where one collects and measures the inputs and outputs for a specific product for its whole life cycle". The LCI is usually the most time-consuming and complicated stage of the LCA. The aim and scope directly influence what type of LCI technique is suitable. Choosing the proper LCI technique is crucial as it can lower costs and the complexity or time involved. (Islam et al., 2016)

2.1.1 LCI methods

There are numerous LCI methods available, and more are being developed constantly. However, the three main LCI methods available presently are the "Hybrid method", "Process-based modelling", and "Input-output (IO) LCI". Each process possesses various advantages and disadvantages and must therefore be carefully chosen to suit the specific application. (Islam et al., 2016) The first LCIs performed in the 1960s utilized the process-based modelling method through a process flow diagram. The process flow diagram shows how the processes of the production systems are linked through commodity flows. The basic layout for a process flow diagram is to set up boxes and arrows, where the boxes represent processes and the arrows commodity flows. Only by utilizing plain algebra can one obtain the number of commodities fulfilling a specific functional unit and multiplying the environmental interventions created for producing them, the LCI can be calculated. (Huppes & Suh, 2005) This LCI method is highly efficient for simple and straightforward product systems, but more often, industrial processes are built up by several input streams and output streams, making the process flow diagram method unsuitable due to allocation problems. (Islam et al., 2016)

The matrix method is introduced to overcome the limitations of the process flow diagram in process-based modelling. The matrix method makes it possible to solve several product systems with a vast number of equations simultaneously. The matrix approach simultaneously solves various linear equations that express the entire product system. It can be used for systems that have, for example, multiple inputs and outputs, internal looping, and recycling. (Islam et al., 2016)

Nevertheless, being a process-based modelling method, it requires much primary and axillary process data, making it time-consuming and even complicated. Therefore, the Input-output (IO) LCI method is preferred by some practitioners, as it can deliver faster and more simple solutions with a more expanded boundary for the system. The IO LCI method derives its values from input-output databases. (Islam et al., 2016)

The IO LCI method works opposite to process-based modelling, as it has a "top-to-bottom" approach and involves macroeconomics. (Crawford et al., 2018) The IO LCI method is widely utilized for various environmental applications and possesses excellent benefits since it considers the entire supply chain in the economy. The greatest downfall of this method is that the IO databases may not reach the level of detail required to perform an accurate LCI. The data might also be outdated. Also, accurate results cannot be attained when the upstream processes are strongly dependent on imports. A hybrid method has been introduced to overcome these challenges in the IO LCI method and process-based modelling. (Islam et al., 2016)

The hybrid method is challenging to define, as it often hybridizes process-based and IO LCI clearly. However, in an attempt to clarify the hybrid

method, the four main methods have been categorized as "Tiered", "Path exchange", "Matrix augmentation", and "Integrated". Figure 2 shows where each hybrid method lies between the spectrum of process-based LCI and IO LCI. (Crawford et al., 2018)

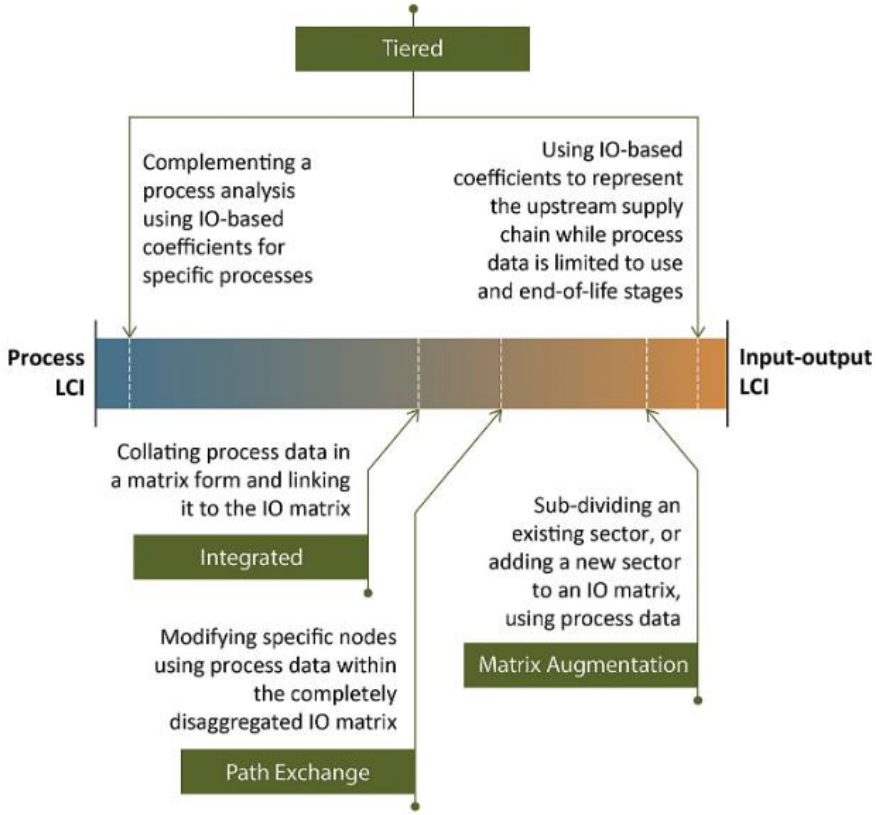

Figure 2, The spectrum of Hybrid LCI (Crawford et al., 2018).

The tiered hybrid method combines coefficients from both process-modelling and IO LCI to expand the system boundary. The path exchange hybrid method involves breaking down an IO matrix, which allows for identifying and modifying matrixes with mutually exclusive pathways. In the matrix augmentation method, the IO matrix is directly modified to generate additional sectors in the economy. Finally, the integrated method involves integrating process-modelling and IO data into one matrix, where vectors (upstream and downstream) connect the two matrices. The main challenge for the hybrid LCI method, in general, is that the processes are still not clear and vary greatly between authors. This creates challenges for future authors to choose the most suitable method and understand potential limitations. Also, hybrid LCI methods often depend on process-modelling and IO LCI methods, which can create similar truncation issues as the original method. (Crawford et al., 2018)

2.1.2 System boundaries

Some of the processes from the LCA will be either included in or omitted from the system according to the system boundary. A process flow diagram illustrating the processes and their connections is useful in describing the system. (ISO 14040:2006, 2006) All of the methods covered in the LCA are presented in figure 3 as a generic process flow diagram within the box designated as the system boundary.

To accurately define the system boundaries, combining a variety of cut-off criteria is frequently necessary. For instance, an extra check should be performed to see if little but extremely effective levels of powerful pollutants and poisons are shut off the system when cut-off criteria set the system limits based on mass. Additional cut-off criteria based on impact can be used to prevent such. (GaBI software, 2011)

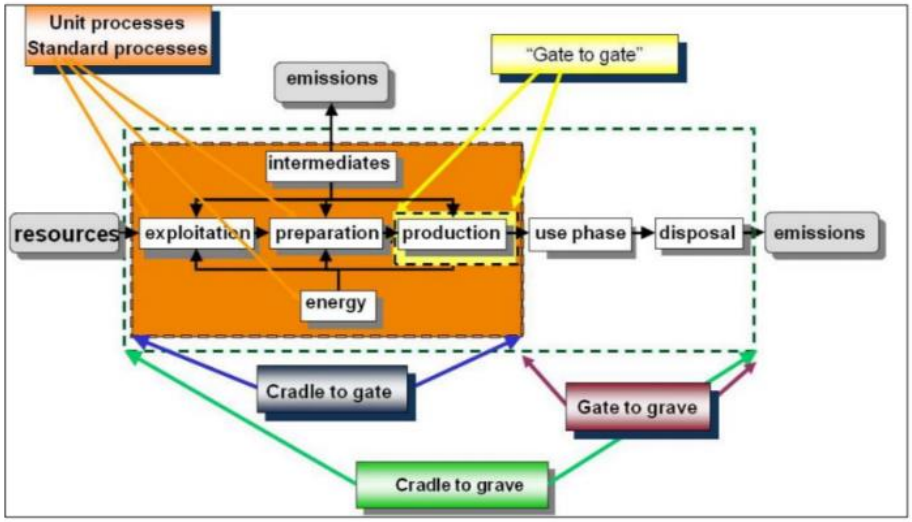

Figure 3, LCA system boundaries (GaBi Software, 2011).

Cradle-to-grave is for all procedures, from the mining of raw materials to the manufacture, transportation, and consumption phase through the disposal of the product at the end of its useful life.
Cradle-to-gate no transportation to customers included, and the LCA is limited until the end of the production, limiting the LCA from raw material extraction only up to production.
Gate-to-grave includes all post-production procedures (everything after manufacturing) used to assess the environmental effects of a product after it leaves the plant.
Gate-to-gate contains just production-related procedures; used to assess the environmental effects of a particular manufacturing step or process. (Reuter et al., 2020)

For this master thesis, the system boundary is "Gate to Gate" since it only studied the production phase of the metal components. A "cradle to gate" LCA will later be performed using LCI results with one of these case components for the GREEF project. Therefore, further explanatory literature survey for the steps of an LCA is excluded from this work

2.2 CNC machining and sustainability

Mechanical machining methods have been used for several decades to make parts from a wide variety of materials. Particularly, the machining of metals and alloys such as copper, brass, bronze, and steel are utilized to manufacture both unique and conventional products. In addition, mechanical machining is the most reliable way to make accurate and complete metal parts. (Reinecke et al., 2016)

The micrometer (μm) level for accuracy and surface roughness might be easily attained with a computer numerically controlled (CNC) mechanism device. Consequently, the first systems to emerge in the field of advanced manufacturing and re-manufacturing were those that combined additive and subtractive functionalities. CNC-machining is also called subtractive manufacturing, as it subtracts material from a feedstock, making the shape desired for a component. The manufacturing method utilized by companies to create parts depends on the characteristic of this part. Sometimes one approach could be more environmentally friendly than the other, depending on the complexity of the component. (Song et al., 2022)

In contrast to other manufacturing methods, CNC-machining enables the production of robust metal moulds. Metals like stainless steel, which possess high hardness characteristics, may lengthen the production process, but once machined, the component will survive longer owing to their hardness. (Malek-Khatabi et al., 2023)

In the developing world, machining contributes around 5 % of the GDP, making it one of the fundamental industrial technologies. Machining has a more substantial indirect impact on product service life and surface integrity. Moreover, it is anticipated that the importance of machining will increase as economic factors result in shorter product cycles and more adaptable production processes. (Zhang et al., 2020) The machining approach has a considerable impact on energy usage in machining operations. Most machining operations carried out in production facilities use electrical energy. Predicting the energy consumption of a machining approach is critical for a manufacturer before a product is created. Analytical models connecting energy consumption and machining approach have been created in various earlier investigations. Their correctness, however, is heavily reliant on the parameterization of these models by specific experiments. (Brillinger et al., 2021)

According to Chandel et al. (2021), manufacturing industries use 30 % of the worldwide energy supply and produce up to 36 % of the world's CO2 emissions. Also, Papetti et al. (2019) state that industrial production is a major cause of pollution, using more than 30 % of primary energy. Thus, attention must be placed on energy efficiency, which consists of two distinct areas: eco-friendly product development and energy-efficient manufacturing. As a result, thorough energy-conscious product design and a low-energy manufacturing approach support government environmental regulation. Finally, the geometrical characteristics and manufacturing energy usage of each component must be unavoidable and optimized case by case. (Al Geddawy & ElMaraghy, 2016)

2.2.1 Spur gear conventional manufacturing

There are several types of ways to manufacture spur gear, but there are a few methods that are employed for mass production of the gear. Gear hobbing is one of the most used processes around the world for the mass manufacture of spur gear. Dudley (2012) presented different ways to produce a spur gear:

- **Gear milling**
- **Gear shaping**
- **Gear hobbing**
- **Grinding**
- **Shaving and Honing**
- **Lapping**

Dudley (2012) explains the method of gear hobbing as; "the process of manually removing the metal between gear teeth using a hob, a threaded and gashed cutting tool. The revolving hob features several rack teeth spiralled around the exterior of a cylinder, allowing it to cut several gear teeth simultaneously" p.100. Using single-thread hobs allows for the finest surface quality. If the gears are shaved or lapped after hopping, the precision gained through hopping becomes less significant. Hobbing can only be applied to generate exterior gears, while skiving, a method like hobbing, is utilized to produce internal gears. (Dudley, 2012)

For this thesis, spur gear manufacturing was carried out with a CNC-machining process called Modular disk milling (gear milling), which uses a module mill tool. According to Sandvik (2022), modular disk milling is a technique for milling the outside gears, splines, and straight bevel gears with unrivalled flexibility, which makes it highly desirable for small batch manufacturing and where short lead times are essential.

A CNC-milling machine executes the approach to produce many gear profiles with the same tool set, as it is shown in figure 4.

Figure 4, Invo-milling of spur gear (Sandvik, 2022).

Modular disk milling inserts in the channel from the gear tooth using the face-cutting tool. A line or interval separating the plane of the tool face defines the contact between the plane of the tool face and the tooth involute. The tool route is generally circular from top to bottom, as shown in figure 4. Hyatt et al. (2014) indicate that "as a result, the tool path, and not the tool itself, determines the critical variables of the gear (module, pressure angle, and helix angle), a trait often associated with flank or ball end milling as opposed to hobbing, gashing, or shaping tools."

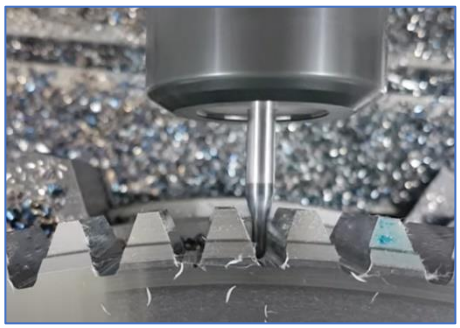

Figure 5, Sandvik spur gear (Sandvik, 2022).

Figure 5 shows a ball end mill tool in a CNC-milling machine from Sandvik for finishing after the modular disk milling.

2.2.2 EDM electrical discharge machining

Electrical discharge machining (EDM) involves using an electrical current that travels from the electrode to the workpiece. Those particles are blown away by the spark when the energy goes through the metal. Each release occurs between the tool and the workpiece at the smallest possible distance, and this process repeats hundreds of times each second. (Rashid & Jahan,

2021) It is necessary that the tool and the workpiece be electrically conductive for the procedure to function. Precisely, the tool cuts away the part of the workpiece that reflects the shape of the tool. (Bigot et al., 2006)

Usually, this is an exaggeration of the actual size of the tool due to the clearance. In order to make grooves in the workpiece, the wire electrical discharge machining employs an electrode consisting of a thin wire of copper or tungsten. The wire is transferred from the feeding coil to the collecting coil to dissipate any heat generated. Thanks to the mathematical control of the machine, intricate shapes may be carved out of metal. For example, spur gears with grooves larger than the diameter of the wire are machined using this method. (Marashi et al., 2017)

Due to the heating of the workpiece during EDM machining, dimensional distortions may arise, necessitating the normalization of the workpiece. In addition, when heat is applied to a workpiece, it causes a HAZ (heat-affected zone) on the cut surface, typically measuring 0.05 mm in thickness. It is occasionally required to remove the HAZ layer entirely to withstand high-stress conditions during final usage. (Steuer et al., 2014)

The EDM process was utilized in this thesis for the removal of the components from the build plate of the SLM 125 HL metal 3D printer.

2.3 AM and powder bed fusion laser beam

Additive Manufacturing (AM) arose because of technological advancements in various fields. As with many manufacturing breakthroughs, improvements in processing power and a drop in mass capacity prices provided for handling large amounts of data characteristics. This was thanks to the modern 3D computer-aided design (CAD) that could model a component within short time periods. Currently, there are ample sophisticated computers and other complicated automated devices, and it might be difficult to fathom how the pioneers battled to construct the first AM machines. (Diegel et al., 2019)

Medical, automotive, aerospace and marine industries are currently operating and researching with AM. Thus, AM is a production technology that allows for complexity and personalization. However, this requires labelling and tracing various pieces instead of mass manufacturing the same kind of parts. Nevertheless, AM provides significantly greater scope for customization and complex geometries than conventional manufacturing. When comparing prices, AM is frequently not less expensive if the shape is intended for mass production and just the manufacturing cost is considered. As a result, repeating the whole product design and examining the economics of the entire product lifetime would be sufficing. AM is rapidly evolving, and new companies are continuously joining the market. (Salmi, 2021)

Powder Bed Fusion (PBF) was one of the first and continues to be one of the most versatile AM techniques, suitable for polymers and metals, as well

as ceramics and composites to a lesser degree. There are expanding machine configurations for fusing powders with various energy sources. The most active field of research is in laser-assisted metal PBF procedures. Laser-Based Powder Bed Fusion (LB-PBF) techniques are gaining popularity as a direct production method in various sectors. (Gibson et al., 2021)

Another name for this process is selective laser melting (SLM), a powder bed fusion technology in which the laser heat melts the powder and fuses it. However, electron beam melting (EBM) is not to be confused with laser-based powder bed fusion. Instead, EBM fuses powder in a vacuum-sealed chamber using an electron beam instead of a laser, like the SLM process. (Soundararajan et al., 2021)

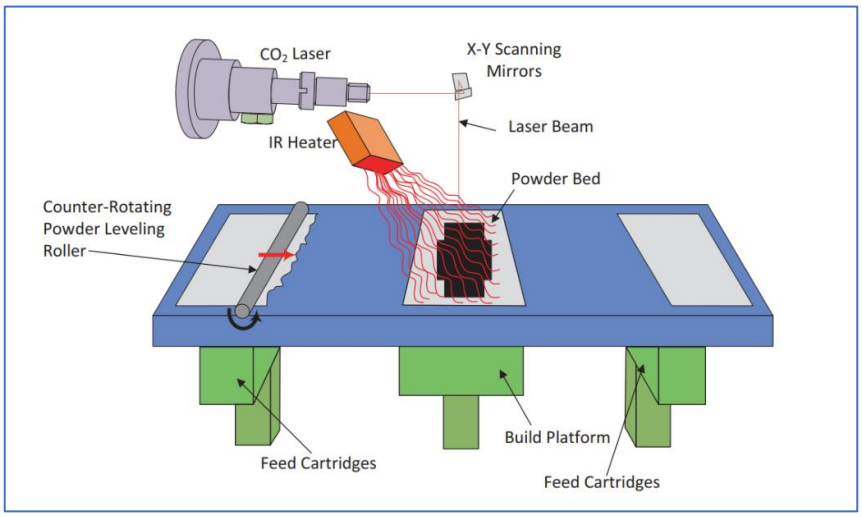

Figure 6, Schematic of the SLS (Gibson et al., 2021).

Figure 6 shows that underneath the laser, there is a melt pool of the metal powder where the metal vapour is enclosed in the chamber. The chamber is filled with inert gas, like argon gas, to reduce the amount of oxygen, preventing oxidation in the high heat of the melt pool. Inside the machine chamber, there are sensors to restrict the oxygen concentration to 1,000 parts per million (ppm). However, this inadequate amount of oxygen is sufficient for the powder to absorb oxygen. Argon gas acts as a stabilizer, and the increase of oxygen affects the hardness and strength of the materials. If oxygen remains in the chamber, the material will decrease in ductility, and fracture toughness will occur. (Moghimian et al., 2021)

Inside the chamber of the machine, there is a bed with fine powder with dimensions from 30 to 60 micrometres (µm), in some cases, could be more, depending on the print. The chamber is sealed, and the powder is fed from canisters below the SLM machine. For the SLM 125 HL utilized in this study, the canisters are placed in the top part of the machine. The laser can vary from 200 to even 1000 watts, but depending on the material utilized, the

print will require different amounts of laser power. Once a layer of powder has already been produced, the bed descends one level, and a wiper system adds a second coating of metal powder to the bed in a uniform manner. The wiper system could also be known as a re-coater. The laser then fuses portions of this layer to itself and the layer underneath, and the procedure is repeated. The sections that the laser will be melting the powder would be according to the CAD design of the component to be printed. The chamber is only opened once the printing is finalized and cooled down. The powder left over inside is removed with a vacuum cleaner and a brush, then sieved, and the particles (powder) less than the size of the sieve are reused. For the case of the SLM, the build plate must be removed from inside the chamber, and the operator must use complete personal protective equipment (PPE). Most prints are usually cleaned with an ultrasonic cleaning machine to remove powder before handling. (Faludi et al., 2017)

2.3.1 Argon gas

PBF-LB machines operate in an environment of inert gas, often argon or nitrogen. (Moghimian et al., 2021) Peng et al. (2020) explain that "argon gas acts as protective gas that prevents metal oxidation during the printing process, and each build consumes approximately 10 L of argon gas". Argon is the noble gas with the highest abundance in the atmosphere of the Earth. It makes up 0.94% of the air, making it the third most abundant element in the atmosphere, after oxygen and nitrogen. (UCAR, 2022)

Argon is also present in trace amounts in the crust and ocean waters of the Earth. Argon is a noble gas, 1.38 times as dense as air and possesses low ionization energy. Its mass determines its capacity to safeguard the melting bath during 3D printing. Argon is primarily derived from the decomposition of potassium in the crust of the Earth. It is an inert gas that does not react with other chemical substances. (Nippon Gases, 2020)

There are many stages of producing argon gas. Even if argon is usually derived as a by-product from a cryogenic air separation unit (ASU), it still requires several more steps to reach the required purity of the Argon. The main challenge for producing high-purity argon is to eliminate nitrogen from it. Extracting argon from the air requires mainly liquefaction and fractional distillation. (Pessoa et al., 2013) The air compressor in a cryogenic ASU consumes the majority of energy. (Aneke & Wang, 2015) These processes are highly energy-demanding, and a future LCI must consider the production of argon gas, as it influences the result of the LCA. For example, Faludi et al. (2017) measured the consumption of argon gas during metal 3D printing of a component with the SLM process and estimated 208 cubic decimetres for each build operation. In the study, it is also emphasized that during the SLM process, all the argon gas is lost after printing. These values could be high depending on the number of parts printed, the size of the chamber and how

the measurements of the argon gas consumption were performed in the study.

Considering the possibility of a future LCA with the data gathered in this LCI thesis, the author of this thesis contacted argon gas manufacturers for information about their embodied energy during production. Woikoski Oy has replied to the request of the author with some values. According to Woikoski, the ASU manufacturing method utilizes 0.19 MWh/Tn. However, the author does not know the output energy measurement techniques for these values provided by Woikoski. Therefore, more information about the embodied energy for manufacturing argon gas must be found to have an adequate LCA of metal 3D-printed components.

2.3.2 Metal powder manufacturing

In recent years the Powder Metallurgy (PM) manufacturing process utilization has increased, producing different types of components. In North America, the experimental studies for PM started in the 1930s, opening the road for the production of PM stainless steel components by the end of 1940. The utilization and manufacture of PM stainless steel parts have increased since then. Among ferrous alloys, stainless steel is well-known for its corrosion resistance, creep, and high-temperature applications. (Pramanik & Basak, 2015)

Controlling the essential qualities of the powder is crucial for producing high-quality stainless-steel components with PM. The size, shape, and configuration of the powder particles and how it is distributed must be taken into consideration. Hence, powder manufacturers must guarantee a good quality of the powder and, at the same time, be regulated to make powder the most cost-effectively and efficiently possible. (Pramanik & Basak, 2015) However, it must be considered that the quality of the powder may degrade with time owing to oxygen absorption and subsequent oxide production in the microstructure. (Hajnys et al., 2020)

Depending on the techniques applied for manufacturing the powder, the higher the total energy consumed would be. Some processes use water atomization to produce irregularly shaped powders. For the production of stainless-steel powders, this system is employed, and also it could be compressed cold, known as compressed grade powders. (Pramanik & Basak, 2015)

Figure 7 shows an example of the material life cycle for powder manufacturing. Starting from the mining stage and completing a whole round after recovering the metal scrap and recycling. Figure 7 is represented with icons of the energy usage and emissions released at every step. In this thesis study, the LCI focus on the product manufacturing phase. This process requires energy and material for manufacturing. The material is the feedstock documented in kilograms of steel that also generates waste.

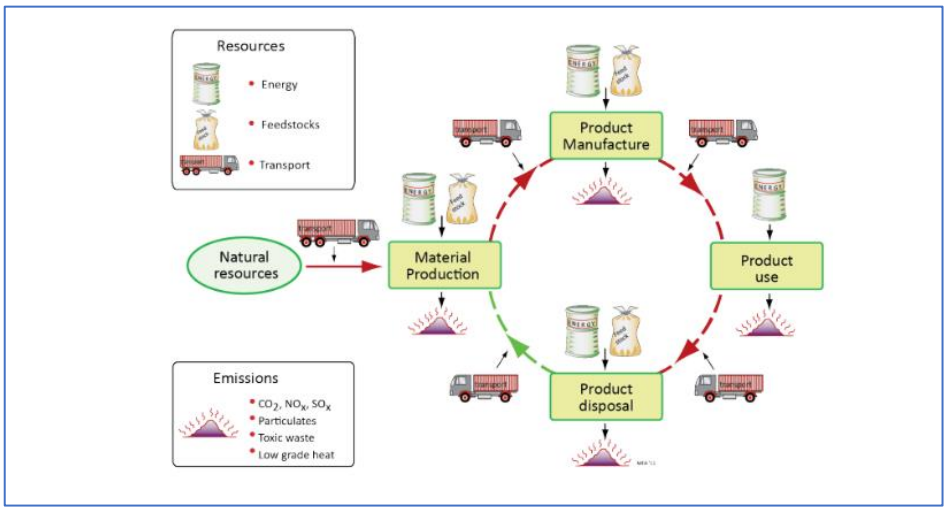

Figure 7, Powder material LCA, Granta Edupack (Ashby et al., 2021).

Figure 8 shows the CO2 embodied in the material for metal powder manufacturing. The stainless-steel bar at the top shows that it requires more energy for the primary production of the metal than for the metal powder manufacturing. The chart bar was generated in Granta software, and it is unknown which atomization process was performed for the metal powder forming. (Sice et al., 2021)

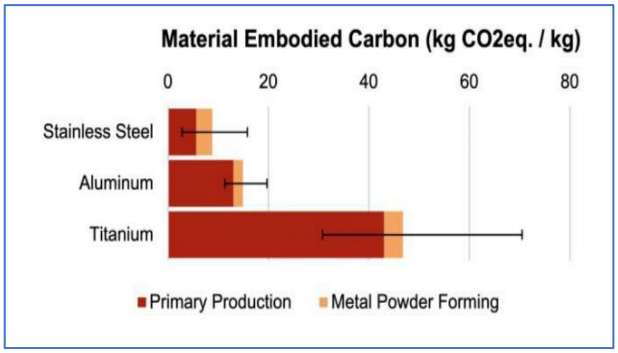

Figure 8, Embodied carbon footprint of metals (Sice et al. 2021).

In conclusion, it is essential to measure the energy consumption for the primary production of metal and for the metal powder forming in order to execute a reliable LCA.

2.3.3 Gas atomization

Gas atomization is the process of creating the metal powder to be utilized in the SLM 3D printer. First, the molten metal is atomized using gas atomization by firing a stream of pressurized gas, liquid, or plasma at the metal as it falls into a chamber, as shown in figure 9. This atomization disperses the particles into smaller droplets, solidifying as they fall into spheres. (Böckin & Tillman, 2019) Initially, small billets of metals are placed inside the argon-filled melting chamber. The melted stream hits a flow of argon stream moving at high speed. The particles are broken into minuscules size, and they are cooled down rapidly for their solidification. Finally, all metal powders are transported to the collecting chamber, as shown in figure 9. (Peng et al., 2020) Another study found that 99.5% of the material becomes powder when atomizing the melted metal, and the rest of the 0.5% remains in the collection chamber walls and filters. (Hajnys et al., 2020)

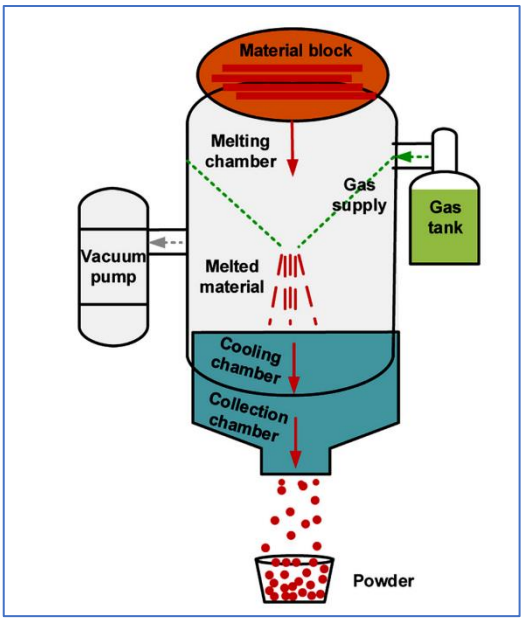

Figure 9, Scheme of the gas atomization process (Peng et al., 2020).

An important point to emphasize is that from the 99.5 % of the material collected, not all the material can be used as a feed powder in the SLM process. For the SLM process, it is only possible to use particles from 15 to 63 µm. A further cause for this is due to the particle size obtained from the gas atomization varying from 1 to 500 µm. For instance, for the powder manufacturers, in order to sell their powder, they have to sieve it, and particles below 15 µm and above 63 µm are sieved out. It is unknown for now if the powder that is sieved out is reutilised back in the chamber to be atomized again or if it is sold for other purposes. From the whole gas atomization batch, around 50-60 % is the usable size for the SLM machine. (Reijonen, 2022) The process

of atomization requires electricity as its energy source. Peng et al. (2020) found in their study that the average energy required to power all the machines involved in making the powder was 60 kW. Additionally, in the study, it was discovered that the gas atomization process had a specific energy consumption (SEC) of 2 kWh/kg of powder produced. These exact values were not collected by the authors of this study but rather by a third party. During the atomization processes, the resources consumed were water and argon gas. The total water consumed to cool down the melted powder was 280 L/kg. However, the study does not state whether the water was recycled or wasted afterwards. Peng et al. (2020) also describe utilizing high-pressure argon gas to fragment the melted metal into powder-size particles, and also argon gas was utilized to avoid oxidation of the metal inside the chamber. In that case, the study states that the argon gas was not recycled, and its consumption would vary depending on the different methods applied. Finally, the study concluded that the argon consumption for gas atomization ranged from 1.5 Nm3/kg to 10 Nm3/kg. On the other hand, Böckin & Tillman (2019) stated that the argon gas consumption for their gas atomization is 3.5 Nm3/kg. All these scientific reports are essential data from the point of view of generating an LCI for a future LCA, and the study concluded with similar or approximate values. However, it is necessary to state clearly the methodology used for measuring argon gas, water, and electricity. There are different kinds of atomization processes for manufacturing metal powder, as shown in figure 10.

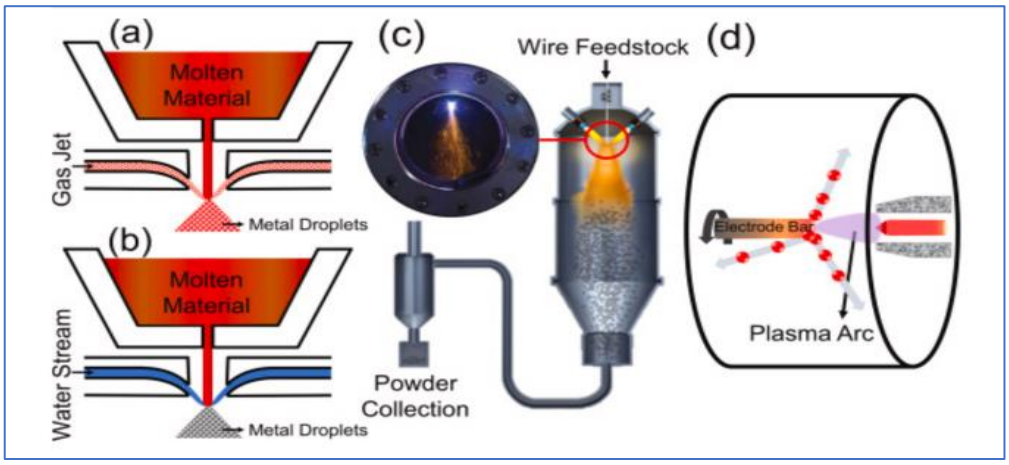

Figure 10, Four atomization methods (Moghimian et al., 2021).

Figure 10 Moghimian et al. (2021) shows the diagram pictures of four different methods for atomization metal powder manufacturing:
"(a) gas atomization, (b) water atomization, (c) plasma atomization with a snapshot of a pre-alloyed wire getting atomized at the apex of plasma torches and (d) the plasma rotating electrode process (PREP), which is a centrifugal atomization process".

It is important to remember that argon is used as a shielding gas and is constantly depleted throughout the atomization of the gas. The extraction method for argon from the air has a significant effect on the surrounding ecosystem. Therefore, it is reasonable to see whether it can be reduced the ecological footprint by better utilization of argon in gas atomization. The studies from Peng et al. (2020) show that the large amount of argon concentration employed in the atomization process is one of the hot spots in an environmental impact. Therefore, when varying the powder preparation techniques, it will require notably different amounts of kilograms of argon gas for every different atomization process. Making the most of this resource is one way to decrease the environmental impact throughout the lifespan of a product. (Peng et al., 2020) In conclusion, powder manufacturers could aim to develop a closed loop for recycling the gas during the atomization and the water used for the cooling. Thus, scientific studies with direct and transparent measurements of the energy and raw material consumption during powder atomization are required.

2.4 Design for additive manufacturing

Design for additive manufacturing (DfAM) is the process through which product designers attempt to produce a design for a product that makes the most of the distinct advantages offered by AM. Additionally, DfAM considers the specific process limitations of the product manufacturing process when utilizing AM technology. This involves more than just modifying components that currently exist in order to accommodate additive manufacturing. Rather it conveys a methodology utilizing the thought process set-on design during the first sketch from the start of the development of a product. (Diegel et al., 2019)

The sustainability of a product can be ensured in the product development phase. It is good to consider several sustainability characteristics that imply AM. For example, Eco design for additive manufacturing (EDfAM) considers designing and manufacturing parts in a way that consumes the least energy and thus releases the minor emissions possible. (Yi et al., 2020)

Currently, PBF and AM are utilized to minimize resources and provide possibilities for lightweight components utilizing design with topology optimization. (Javaid et al., 2021) Topology optimization can create complex geometries. The optimization can create cell-like structures that are biologically inspired, creating components that are lighter in weight than those manufactured with traditional manufacturing. There are different types of topology optimisation that involve modifying the solid body to diverse structures like trusses, lattices, cellular, and mesh. (Diegel et al., 2019)

The lattice can be designed in a variety of possibilities, for example, as a lattice pattern or cell. There are a variety of options for the shape and size of such lattice cells, and this style is reproduced on the part. In addition, several

examples of lattice structures are now being employed in order to either increase the strength-to-weight ratio of a component or to replace support material inside a component. Both of these goals may be accomplished by reducing the quantity of material that is needed. (Diegel et al., 2019)

Ramadani et al. (2018) studied topology optimization for lightweight and low-vibration gear body, in which "a solid gear body was replaced by a lattice structure, which was expected to raise the torsional compliance of the body". In the study, a gear was manufactured with the SLM process with titanium alloy Ti-6Al-4V. The solid gear weight was 0.401 kg, and the optimized lattice structure was 0.255 kg. This means that the lattice structure was 36 % lighter weight than the solid gear.

AM-enabled light-weighting results in improving the use-phase effects; those impacts account for most of the total lifespan impacts in a component utilized for transport applications like commercial aeroplanes. (Sice & Faludi, 2021) Some papers talked about how the product is used. By making parts lighter with AM, environmental impacts in aerospace applications in the use phase were cut significantly. (Van Sice & Faludi, 2021)

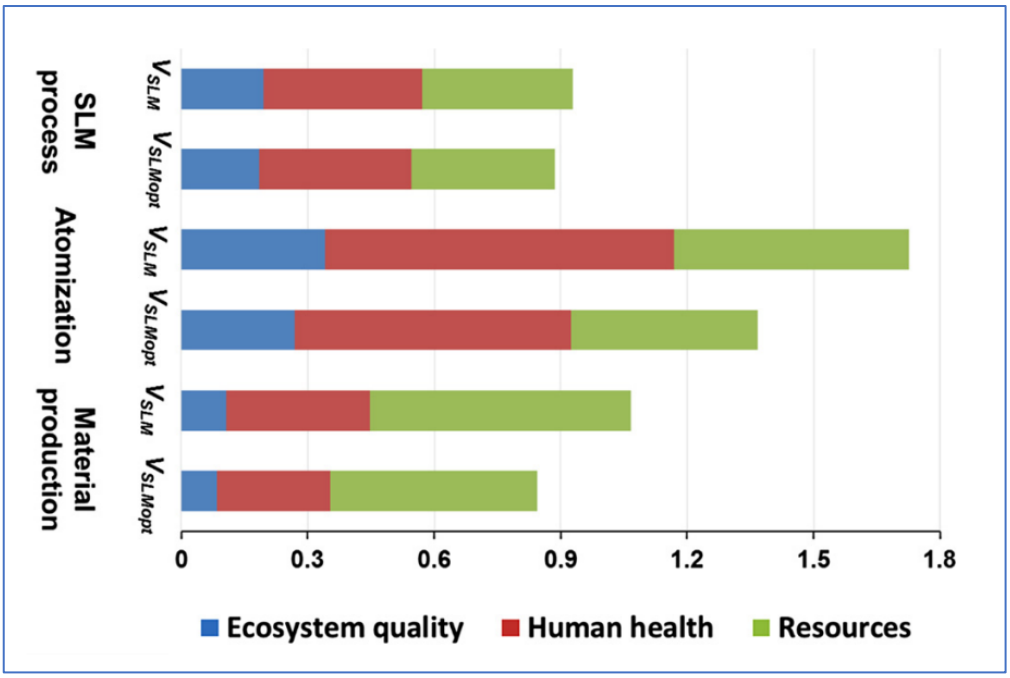

Figure 11, Environment impact comparison of SLM (Peng et al., 2020).

Figure 11 shows a valve manufactured in SLM and optimized and another valve manufactured in SLM with no optimization. (Peng et al., 2020) It is visible that the SLM-optimized valve has a lower environmental impact on the material production, atomization and during the SLM process. This means that 3D prints with the SLM process as an optimized part vs a normal part have lower environmental impacts in three categories: ecosystem quality, human health, and resources (for production).

2.5 Previous comparisons of AM & CM

Additive manufacturing has different types of processes, as well as conventional manufacturing, does. It is complex to make a straight comparison between AM and CM, for this would be necessary to produce the same component with every method for AM and CM and measure the same values. Nevertheless, there is existent literature that compares some methods from AM with some methods of CM during the life cycle of the component. Figure 12 shows the results of an LCA comparing AM methods and CM methods. From AM methods, it was utilized: binder jetting (BJ), bound powder extrusion (BPE) and powder bed fusion (PBF). (Deboer et al. 2021)

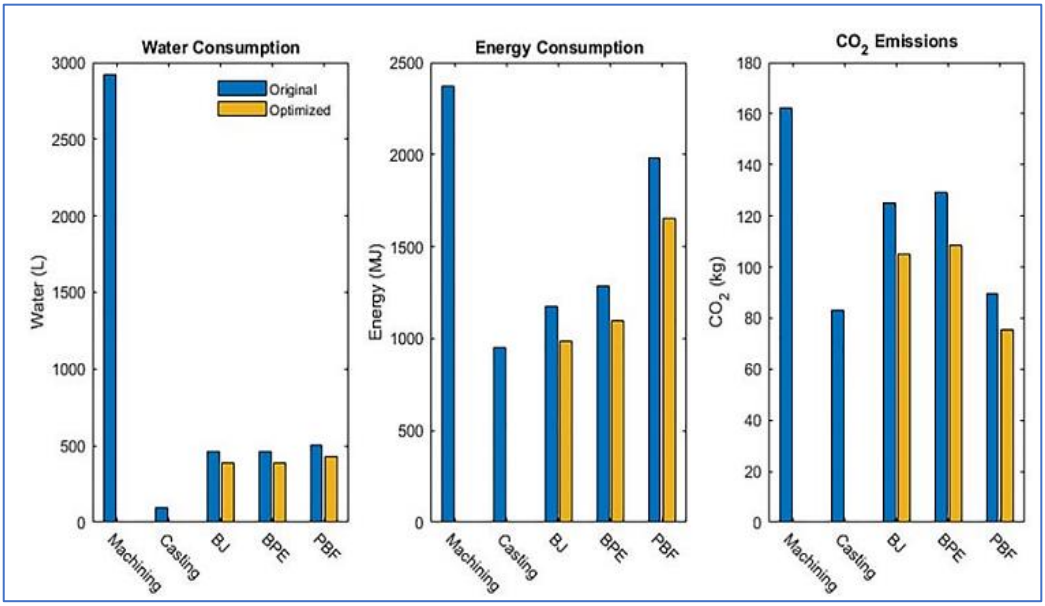

Figure 12, Environmental impact per manufacturing method of an H-yoke (Deboer et al., 2021).

Figure 12, Deboer et al. (2021), shows that the water consumption for the machining utilized 3000 litres for the part to be manufactured. PBF utilized less than 500 litres of water for the same part. The total energy consumption of machining was 2450 MJ, while the total energy for PBF consumed was 1900 MJ for the optimized and 2000 MJ of electricity for the same component. For the CO2 emissions, machining utilizes 160 kg of CO2 for manufacturing and PBF 90 kg/CO2. For this research, CNC-mill was utilized for the machining operations. In Figure 12, it is possible to see the difference between the optimized part and the original part. The optimized part has lower environmental impacts in the three categories: water consumption, energy consumption and CO2 emissions.

Huang et al. (2016) studied that the vast majority of energy savings result from the lower utilization of aviation fuel as a direct result of the lower weight of AM components. Thus, due to the lower need for raw materials, incorporating AM parts into aeroplanes might result in substantial energy savings. In addition, the resources that are required for manufacturing are a contributor to the rise in cost. These resources aid in improving the fuel economy, and that is a consequence of reducing the weight of the components. The weight reduction in that study focused on the structural, auxiliary, and functional components of the aeroplanes. Lightweight materials such as Al alloy, Ni alloy and Ti alloy with AM were combined to achieve weight reduction. The study also added that the aircraft mass could be reduced by up to 17 % when utilizing components manufactured with AM. The study concluded that a decrease in the overall weight of the aeroplane might save fuel consumption by as much as 6.4 %, making this an important goal for the aviation industry. (Huang et al., 2016)

Case study component analysis data (Munsch et al., 2012; Krailling and Novi, 2014; The SAVING project, 2009; EOS, 2013; Tomlin and Meyer, 2011).

Case study component	Material	Original CM pathway	AM technology	Original CM component mass (kg)	Replacement AM component mass (kg)	Mass reduction (CM-AM)/CM
Bracket	Ti alloy	Machining	EBM	1.09	0.38	65%
Seat buckle	Al alloy	Forging and machining	SLM	0.16	0.07	55%
Bionic bracket	Ti alloy	Machining	EBM	0.06	0.04	35%
Engine cover door hinge	Ti alloy	Casting and machining	DMLS	0.92	0.23	65%
Fork fitting	Al alloy	Casting and machining	SLM	0.8	0.4	50%

Figure 13, Weight reduction in components (Huang et al., 2016).

Figure 13 shows the weight reduction increment when producing a component with AM. The last row in the table is a fork fitting made of Al alloy. For CM was made by casting and machining, and AM was executed with the SLM process. The original part weight was 0.8 kg, and the replacement part weight was 0.4 kg. The total mass reduction for the fork fitting was 50 %. Correspondingly, for the engine cover door hinge, the reduction of mass when utilizing AM was 65 % lighter. Similarly, the seat buckle made of Al alloy in the SLM process achieved a weight reduction of 55 %. (Huang et al., 2016)

Energy saving and CO_2e reduction ranges, by adoption scenario.

Year	Projected primary energy savings (million GJ/year)			Projected CO_2e emissions reduction (million t CO_2-equivalent/year)		
	Slow adoption	Mid-range adoption	Rapid adoption	Slow adoption	Mid-range adoption	Rapid adoption
2020	0.001–0.002	0.005–0.015	0.03–0.09	0.0001–0.0002	0.0004–0.0012	0.002–0.007
2025	0.03–0.07	0.2–0.6	2–5	0.002–0.006	0.02–0.04	0.15–0.38
2030	0.3–0.7	3–7	32–65	0.02–0.05	0.2–0.5	2.4–5.0
2035	1–3	13–27	38–78	0.1–0.2	1.0–2.1	2.9–6.0
2040	4–8	28–59	60–145	0.3–0.6	2.1–4.6	4.6–11.2
2045	8–19	43–97	66–163	0.6–1.4	3.3–7.4	5.1–12.6
2050	16–36	56–134	70–173	1.2–2.8	4.3–10.3	5.4–13.3
Cumulative (2019–2050)[a]	**110–250**	**598–1339**	**1195–2789**	**8.5–19.3**	**46.1–103.4**	**92.1–215.0**

[a] Units for cumulative savings are million GJ and million t CO_2-equivalent.

Figure 14, Energy saving and CO2 reduction ranges (Huang et al. 2016).

Figure 14 shows the total potential for primary energy savings in the scenario of rapid adoption. This energy level will reach 70 to 173 million GJ/year by 2050, with primary energy savings reaching between 1.2 and 2.8 billion GJ. (Huang et al., 2016) The general energy and carbon reductions achieved by 2050 via AM components in aeroplanes might be far greater if the technology were embraced sooner. To produce parts that can be accepted fast, several technical obstacles, such as the issues of machine output, geometric repeatability, residual stress, and rough surface, must be resolved. (Huang et al., 2016)

In conclusion, some effects of AM and conventional CNC-machining may be compared directly, while others cannot. Both utilized substantial quantities of energy, as previously shown. In all instances, the energy consumption is mostly influenced by component shape or finish quality via their impacts on processing time. (Faludi et al., 2015)

3 Materials and methods

This chapter aims to define effectively the components utilized in this thesis that were utilized for measuring energy and material consumption. As well as to describe the employed machinery and materials characteristics. The components were 3D printed with several parameters, which are explained in this chapter.

3.1 Description of the components

For this thesis, three different components were utilized to measure the energy and material while 3D printing and CNC-machining. As mentioned in chapter 1.3, the CNC-machining was performed at Oulu University machine shop with a CNC-lathe and CNC-mill. The 3D-printed parts have been manufactured at the VTT's AM laboratory with SLM PBF-LB. All the 3D printed parts were sent to Oulu University for post-processing, thread making and support removal. Some machining parts were produced with different types of steel. Table 1 illustrates the names and materials of the components.

Table 1, Components names and materials utilized for each method.

		The material utilized for each method		
Company	Component name	SLM 3D print	CNC lathe	CNC mill
VTT	Spur Gear	SS316 L powder	no lathe	SS316L
SEW	Manifold	SS316 L powder	11SMn30+C	11SMn30+C
Proventia	Impeller	SS316 L powder	no lathe	SS316L

Table 1 shows that the spur gear and impeller components have been produced only with a CNC-mill and that the manifold has been produced both with a CNC-lathe and a CNC-mill.

Table 2, Number of parts CNC-machined at Oulu University.

Company	CNC Machined at Oulu	Type of machining
SEW	Manifold	LATHE
SEW	Manifold	MILL
Proventia	Impeller	MILL
VTT	Solild spur Gear	MILL

Table 2 shows that the manifold has been machined twice. This was completed for a better comparison in the LCI. One manifold was manufactured with the CNC-lathe and another one with the CNC-mill.

The following table 3 explains the number of components printed per build. Due to the size of the parts and the build plate, for some components, more than one could be printed at a time. For example, in the build plate, it is possible to print four-manifolds at once. This aids in having a more comprehensive comparison of the LCI.

Table 3, 3D printed components at VTT with SLM 125 HL.

Company	SLM parts per build at VTT	Method
SEW	4X Manifold 30 µm	SLM
Proventia	1X Impeller 30 µm	SLM
Proventia	1X Impeller 50 µm	SLM
VTT	2X Lattice gear 30 µm	SLM

Table 3 shows that the lattice gear is printed twice since it was possible to place two gears flat in one build plate. However, for the impeller, only one component fits in the build plate per print. Therefore, two different prints have been made with two different layer thicknesses of 30 µm and 50 µm.

The following table 4 explains the 3D-printed components sent to Oulu for machining. The manifold part has threads in the holes, so it must be machined, and the energy was measured from those operations.

Table 4, 3D printed components post-process machined at Oulu University.

Company	CNC finished at Oulu	Type of machining
SEW	4 Manifolds	MILL
Proventia	2 Impellers	MILL
VTT	Lattice spur Gear	MILL

Table 4 shows that the lattice spur gear and the impeller have been sent to Oulu University to remove the extra material and final finishing operations. These post-processing operations were performed with the CNC-mill.

3.1.1 Manifold

The manifold was provided to VTT by SEW Industrial gears Oy, an industrial gearbox manufacturer. SEW is located in Karkkila, Finland, and is owned by SEW-EURODRIVE in Bruchsal, Germany. To better satisfy the global need for diverse industrial gear systems and components, SEW has increased the range of its products. The company's current vision is defined as follows: "An agile industrial gear solution and technology provider to EURODRIVE's customers for the entire lifecycle." In order to optimize the design and production process, the firm has planned an investment program while considering the need for sustainable development. The diverse support offered by SEW's

GREEF R&D project will help the transformation process go smoothly in the ensuing years. The project offers the researcher a top-notch research object to generate a study using the data. (SEW Eurodrive, 2022)

Characteristics of the SEW manifold:

The main functionality of this manifold is that oil enters from one end and has a pressure valve at the other end. The universal plugging or feedings makes it suitable for different gears. The pressure for the small holes is up to 2 bar. This manifold generally works as an overpressure valve that opens at 10 bar and recycles the oil to the suction side. As a result, a maximum pressure of 10 bar may occur in the splitting supports. In this study, it is machined from a hexagonal bar of steel 11SMn30, and the corrosion resistance, surface quality, and threads are considered.

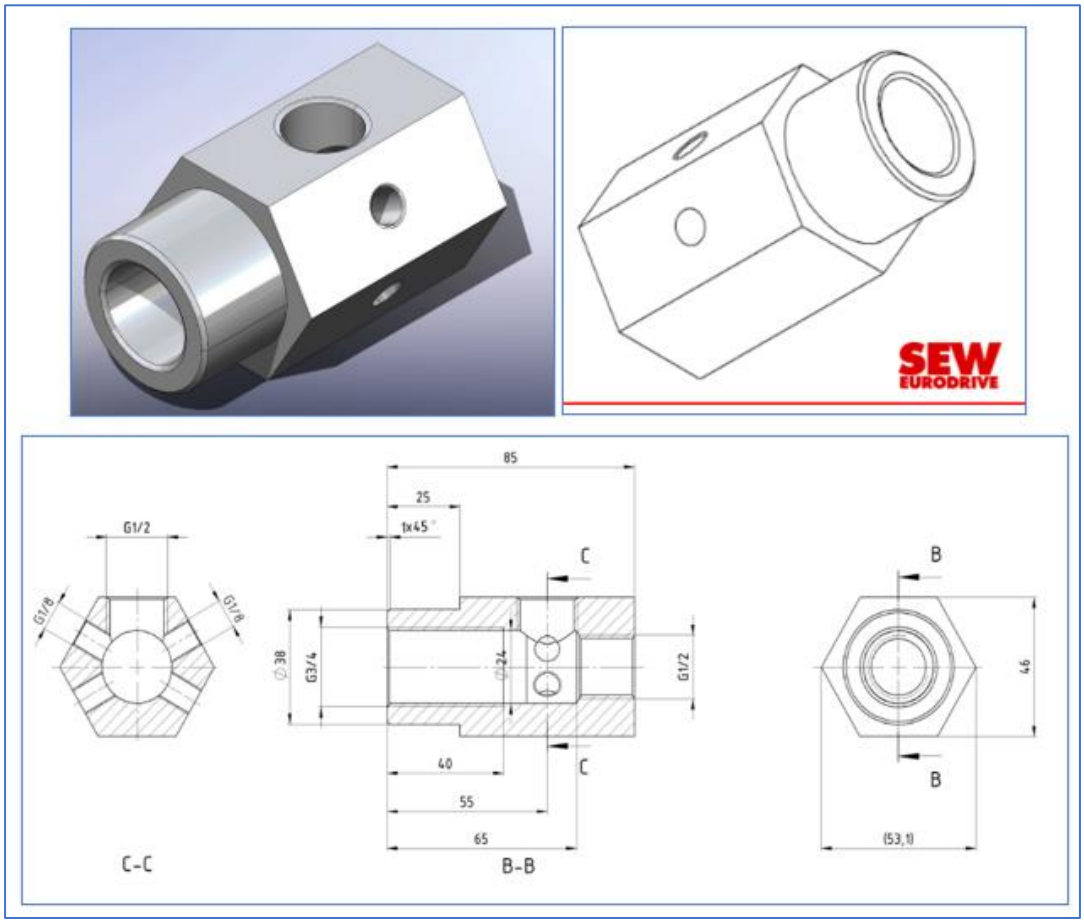

Figure 15, Manifold CAD model and 2D drawing (SEW Eurodrive 2022).

Figure 15 shows the manifold from SEW, and in the top left corner, the CAD model; in the bottom section, the 2D drawings with the specifications with the hole sizes and thread dimensions.

Table 5, Manifold international thread standard units.

Nominal Diameter	Major Diameter (mm)	Minor Diameter Nut	Tapping Drill Size (mm)	Thread Pitch (mm)
G1/8	9.728	8.848	8.565	0.907
G1/2	20.955	19.172	18.633	1.814
G3/4	26.441	24.658	24.120	1.814

Table 5 shows dimensions presented in millimetres from Gewinde Normen (2022). This information was necessary to know in order to prepare the builds in millimetres.

3.1.2 Impeller

The impeller was provided to VTT from Proventia Oy, the head office, for research, development, and assembly of test modules is in Oulu, Finland. Proventia is a technology business that develops and produces systems and components that increase the energy efficiency of powertrains in large machines and vehicles. It provides solutions for the engine, machine, and vehicle sectors. Batteries, electric powertrains, thermal insulation components, and exhaust after-treatment systems. For the development and testing of electric and hybrid cars and their battery packs, Proventia also provides modular test facilities. Products from Proventia aid in the fight against global air pollution and climate change. Proventia is dedicated to minimizing its carbon footprint as well. Proventia aspires to enhance its operations and production under the GREEF project to be carbon neutral by 2035. (Proventia Oy., 2022)

Characteristics of the Proventia impeller

Due to confidentiality and IPR protection, Proventia has asked VTT not to show any 2D drawings, CAD models, or images of the actual component. Initially, it is manufactured with conventional methods from SS 316L, with a diameter of about 100 mm and around 12 mm thickness. Since it is impossible to show the original photos of the component, the author utilized images from Faludi's et al. (2017) article that resembles a similar impeller. It is not intended to mislead the reader from the original component.

The impeller was 3D printed at VTT and machined at Oulu University. The following figure 16 aims to give an idea of the impeller.

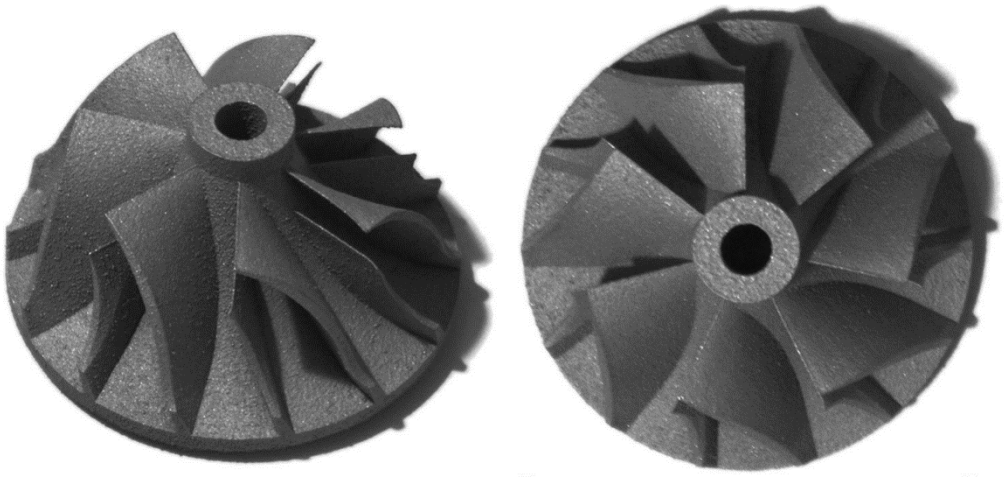

Figure 16, Impeller printed test experiment (Faludi et al., 2017).

Figure 16 from Faludi et al. (2017) describes the image as a "geometrically complex turbine". However, the Proventia impeller and also figure 16 are such that plenty of material removal is needed to manufacture this geometry with CNC-machining.

3.1.3 Spur Gear

The spur gear is the third component used to measure the energy consumption and make a comparison for the LCI. This spur gear has been designed and manufactured in two ways:

- The solid spur gear
- Lattice pattern spur gear

First, the author designed the solid spur gear manually in SolidWorks 2021. The dimensions of the tooth path were given by the Oulu University machine shop accordingly to the required tool dimension available in the machine shop. Then the author designed the lattice pattern inside the solid gear aiming for weight reduction. The solid spur gear was manufactured with a CNC-mill machine with a modular disk milling, as explained in chapter 2.2.2. The traditional way to mass manufacture spur gear is gear hobbing. However, modular disk milling is also used, especially for making prototypes. As explained at the beginning of this chapter, the lattice gear was 3D printed twice in one build. The two lattice gears have been 3D printed at VTT with SLM 125 HL and then sent to Aalto university to detach the parts with the EDM. Finally, the parts were sent to Oulu University for the front mill and tooth path operations. This spur gear, solid and lattice pattern have the exact dimensions; 59 mm in diameter and 8 mm in thickness. The lattice pattern only has less material.

Solid Spur Gear

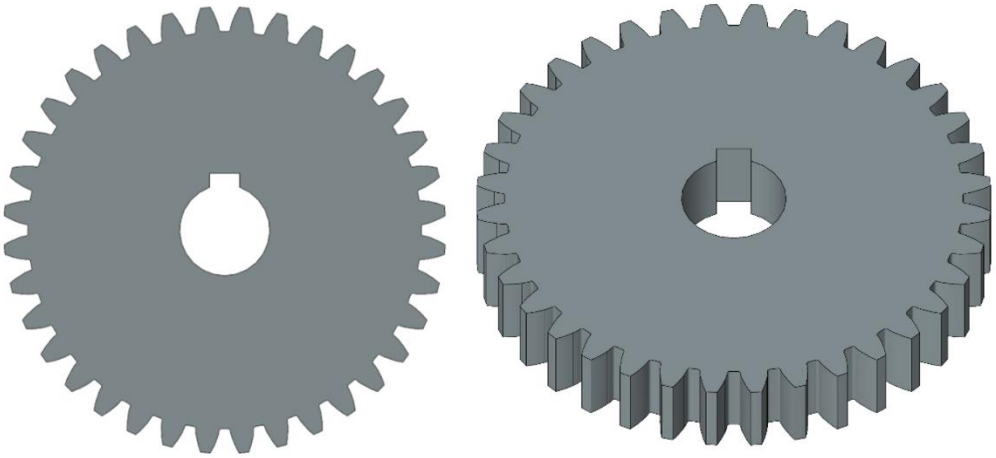

Figure 17, Solid spur gear design in Solid Works 2021.

Figure 17 shows the solid spur gear; in this image, it is observable that the gear has a keyway in the inner hole. The keyway was required when the CNC-machining of the gear was set to be used as a mark. These gears have no real-life functionality, but they were manufactured as if they would.

Lattice Pattern Spur Gear

The author was inspired to make the lattice pattern from a scientific article called: "Topology optimization-based design of lightweight and low-vibration gear bodies" by Ramadani et al. (2018). Figure 18 shows the image from that article with a spur gear with a lattice structure. In order to optimize the lattice structure of the gear body, a software called CAESS ProTOp was applied. This high-performance program topology optimizes with 3D solid finite elements, 3D printed with the SLM process with Titanium alloy material. (Ramadani et al., 2018)

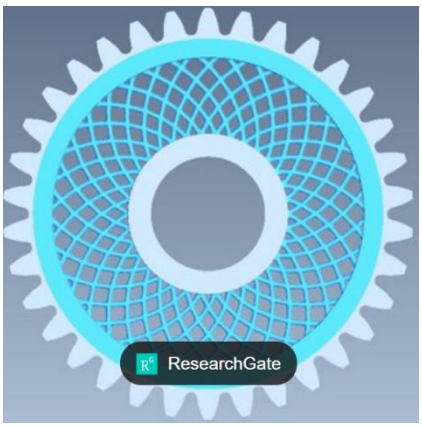

Figure 18, Lattice structure spur gear optimization (Ramadani et al., 2018).

The author of this thesis has designed the inner pattern of the gear, as seen in figure 18. However, the author of this thesis did not make a lattice structure as Ramadani et al. (2018) did, but instead, a lattice pattern.

Figure 19 shows the inside view from the lattice structure, which is a three-dimensional structure, showing the stress concentrations. According to Ramadani et al. (2018), "the lattice structure raises the torsional compliance of the body". Therefore, the gear on the right side of figure 19 is topology optimized and shows less stress concentration than the gear on the left side.

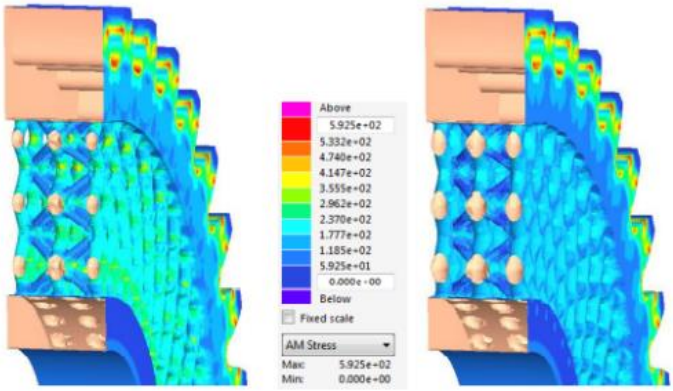

Figure 19, Optimized lattice structure cross-section view from von Misses stress (Ramadani et al., 2018).

Figure 20 shows the spur gear with the lattice pattern made by the author. This lattice pattern and solid gear have a keyway to aiding the machining processes. The gear on the left has added material in the tooth path for 3D printing and then to be CNC-machined. A range of 0.3 to 0.7 mm of material was added to each tooth shown in chapter 3.2.1.

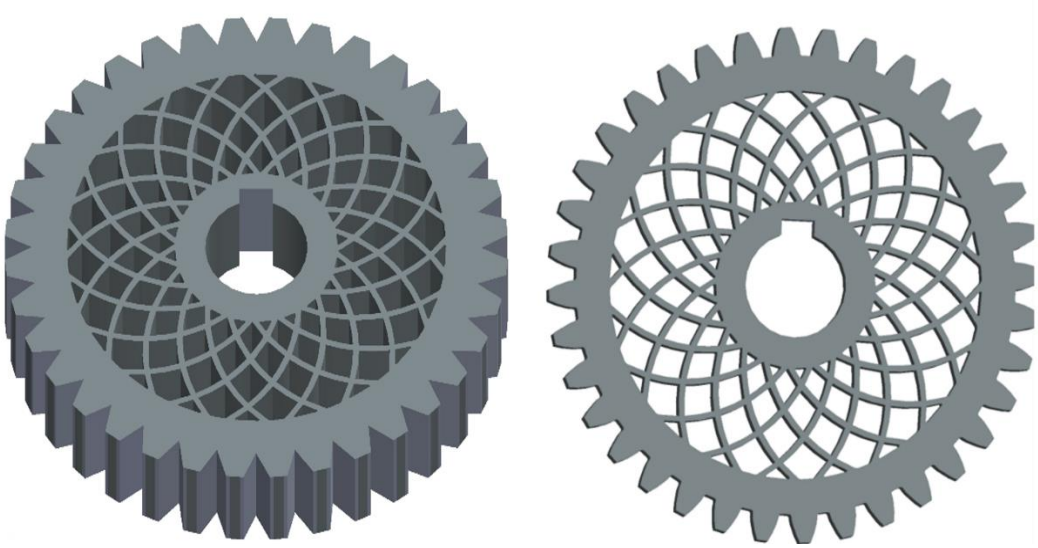

Figure 20, Lattice pattern spur gear design.

Figure 21 intends to show the cross-section view from the lattice pattern spur gear, which is different from a three-dimensional lattice structure. The main difference between the structure and the pattern is that the pattern is filled with material along the width of the gear. In this thesis study, the lattice structure was not utilized in order to avoid using support or prevent failures during 3D printing. Instead, a lattice pattern is used to reduce weight while maintaining the strengths and functionality of the gear.

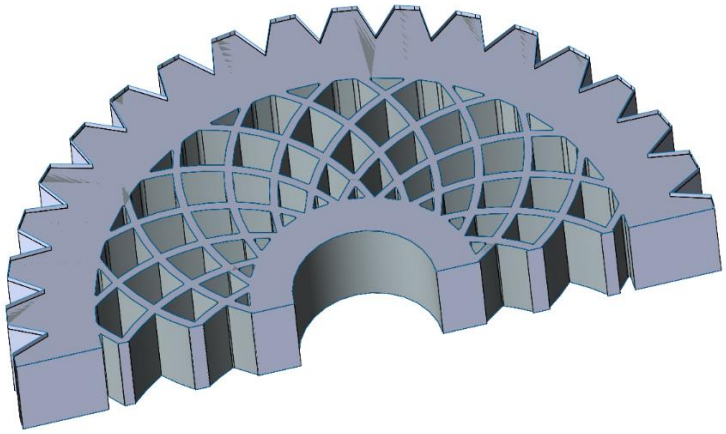

Figure 21, Cross-section view of the lattice pattern spur gear.

3.2 Preparation for metal 3D printing

In order to print the components with the SLM machine at VTT, several tasks needed to be performed beforehand. Once it is decided what part will be printed, changes must be made to the CAD design for the parts to be printable. Finally, when the CAD parts are ready, the builds must be generated with software suitable for the SLM machine.

3.2.1 3D CAD design changes

When a component is printed in an SLM machine, the new part will be welded to the build plate of the machine. In other words, the new part is attached to the build plate and needs to be removed afterwards. Thus, extra material as allowance for the separation must be added to the components before the SLM process. Therefore, the CAD parts must be carefully studied for what would be the optimal orientation in the SLM-build plate. The orientation of the component in the build plate is designed to avoid using excess supports and to determine where and how much extra material will be added. Once the part is ready, the CAD file must be saved as a “. STL" file with customized mesh to be utilized in the build preparation.

Manifold CAD design changes

For the manifold, many changes were made, starting with the big hole in the side. On the left side of figure 22, it is shown the largest hole in the side of the component in the original dimension. In the middle of figure 22, it is shown how the manifold looks after adding 1.56 mm of material. The reason for making this hole smaller was to have enough material when the threads were machined afterwards.

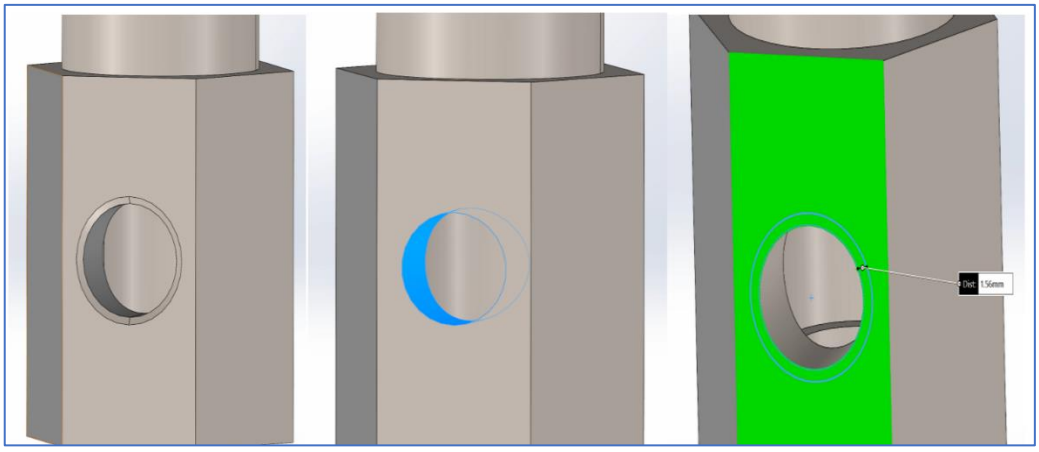

Figure 22, Manifold 3D CAD design changes in the larger hole.

Figure 23 shows that the small manifold holes have been completed, closed, and extruded with material for metal 3D printing. The reason for filling this hole was that material needed to be added for the proper thread dimensions. Another reason was that the software that prepares the SLM files would automatically add support in those holes; hence holes needed to be drilled.

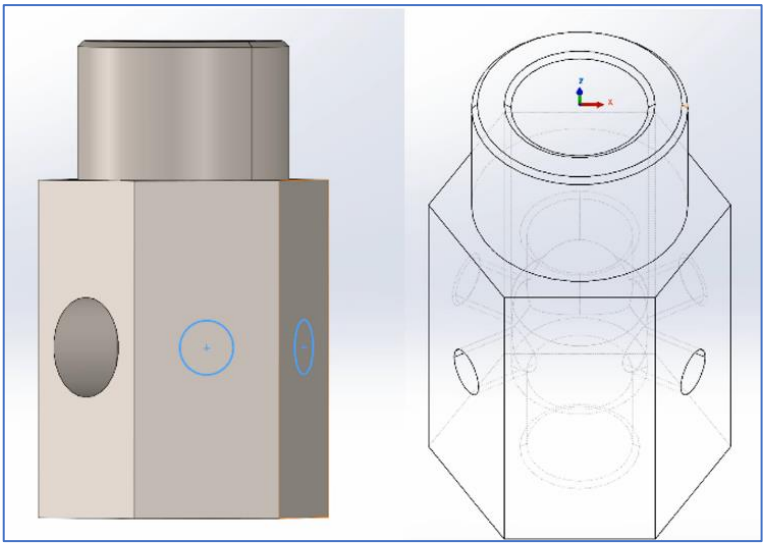

Figure 23, Manifold 3D CAD design changes small holes.

Figure 24 shows the manifold component with 0.75 mm of added and extruded material at the bottom of the part in SolidWorks software. The reason for this was the detachment of the component from the build plate from the SLM 125 HL machine.

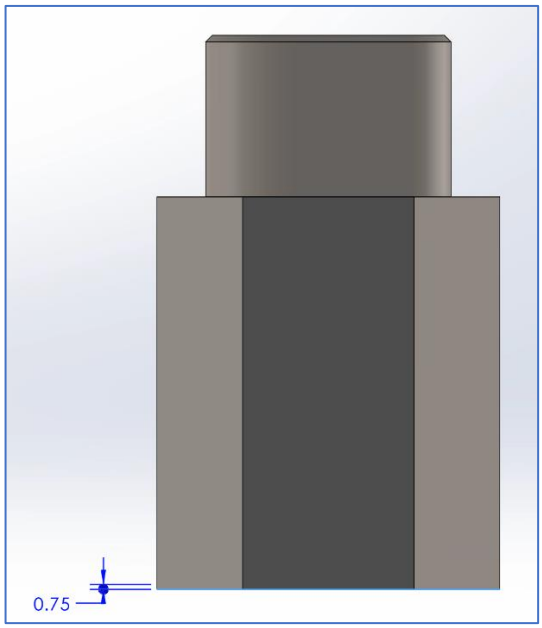

Figure 24, Manifold 3D CAD design changes at the bottom of the part

.

Impeller CAD design changes

For the impeller component, it is impossible to show authentic images of the changes made in the sketch from the original part. Instead, the author has found on GrabCAD website a similar impeller as described in chapter 3.1.2, figure 17. Figure 25 shows a turbo compressor wheel design by Hossen (2022).

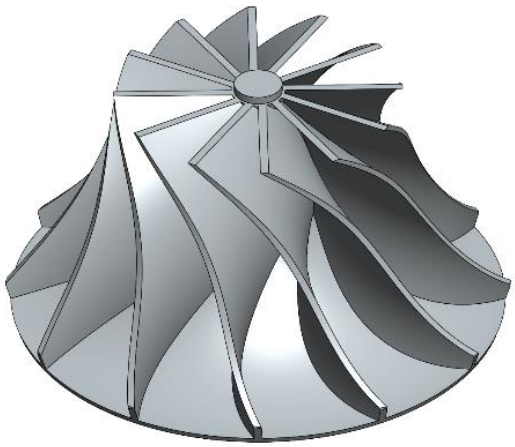

Figure 25, Similar Proventia impeller from GrabCAD (Hossen, 2022).

Figure 26 shows a similar impeller with a sketch in the bottom part of the impeller of 1.00 mm of thickness. This sketch represents where the impeller has been added material as "Boss-Extruded" at the bottom of the part. The reason for adding material in the bottom of the part was to avoid overhang supports and to be able to detach the component out of the build plate of the SLM 125 HL machine.

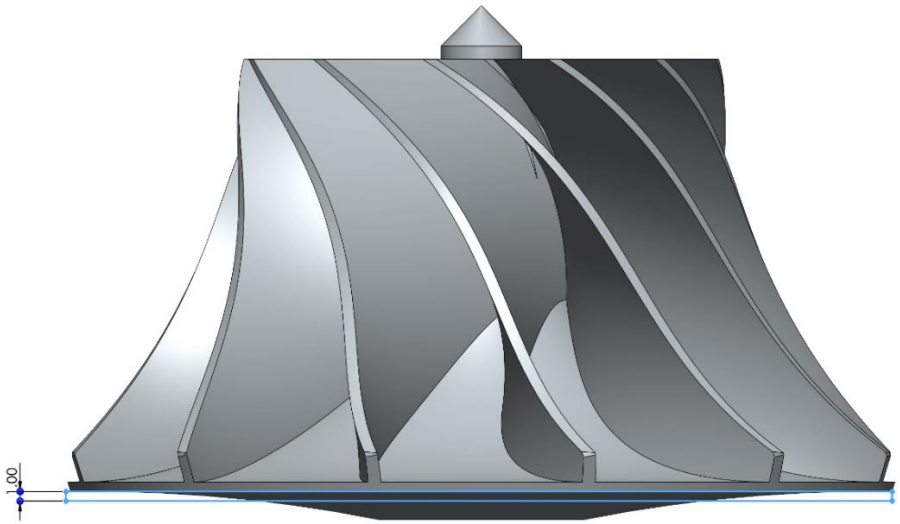

Figure 26, Impeller CAD changes at the bottom of the part (Hossen, 2022).

Spur gear CAD design changes

Only the lattice pattern spur gear has been 3D printed with the SLM 125 HL. Therefore, changes in the CAD design have only been made in the lattice pattern spur gear. Figure 27 shows the extra material that has been added in the tooth path to be machined after that is metal 3D printed. This was to achieve better surface roughness quality and dimension tolerances like an actual spur gear.

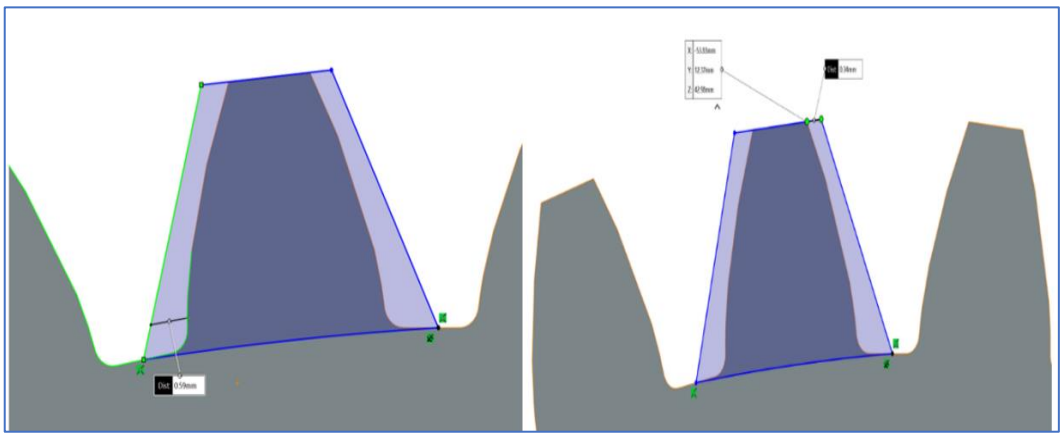

Figure 27, Spur gear tooth path extra material.

Figure 28 shows the thickness of the spur gear on the left side as 8 mm. On the right-hand side of the figure, the spur gear is 8.5 mm. The reason for this was to make the spur lattice pattern gear increase in height when looking from the side because it was printed in a flat orientation. The extra 0.5 mm was added to detach the gear out of the build plate of the SLM 125 HL machine. The reason only 0.5 mm was chosen was to avoid waste of raw material when detaching the part in the EDM machine.

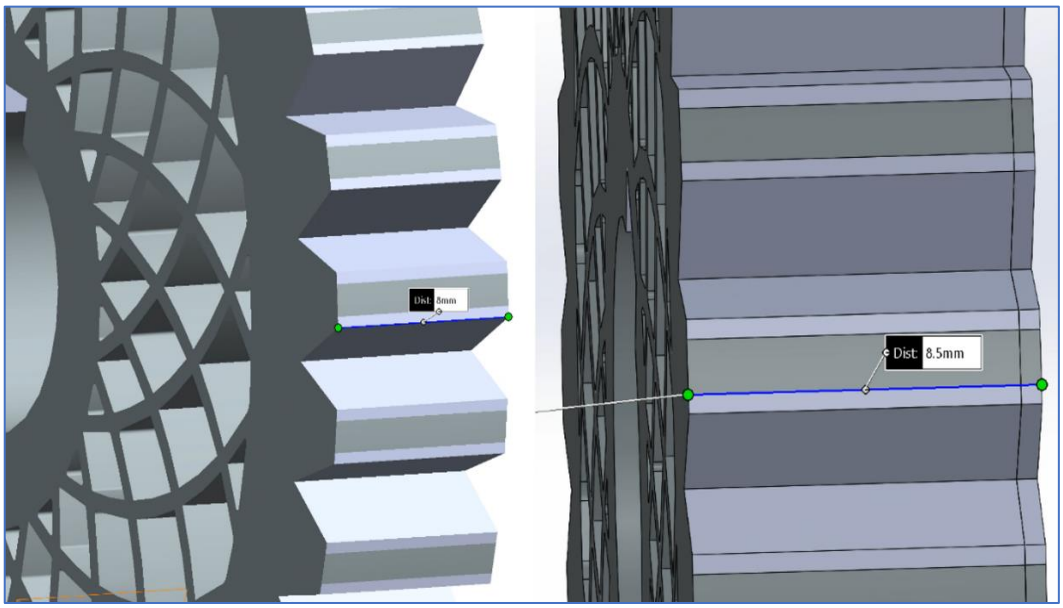

Figure 28, Added material to the Lattice pattern gear.

3.2.2 Preparation of the build for 3D printing

The build preparations were achieved with Magics Materialize software 25.01. This software allows the introduction of a CAD design in an STL format to be placed in the build plate of the SLM 125 HL. Magics Materialize also loads the actual SLM machine parameters and dimensions of the build plate. The parameters for printing the components would vary depending on the material utilized and the layer thickness for printing. The 3D printer manufacturer, SLM solutions, provides those parameters. When the print job is created in Magics Materialize software, the file is saved as a “. Slm”.

In order to check for errors in the (.Slm) file, there is another software called "SLM Slice Viewer" Version 1.0.11. The SLM slicer allows us to visualize the components layer by layer to see if there is any error with the printing vectors. These vectors are made in Magics Materialize from the parameters provided by SLM solutions. The vector contains information such as layer thickness, scanning speed, laser power, hatch distance and many others.

Manifold build preparation

Figure 29 shows two views of the manifold in Magics Materialize software. The original CAD design was modified with added-extra material, saved as a (.stl) file and inserted into the software. As a result, the software can load the exact build plate from the SLM 125 HL with the exact dimensions. In addition, when the supports are added, the software shows them in blue, as shown in figure 30 in the side hole of the manifold.

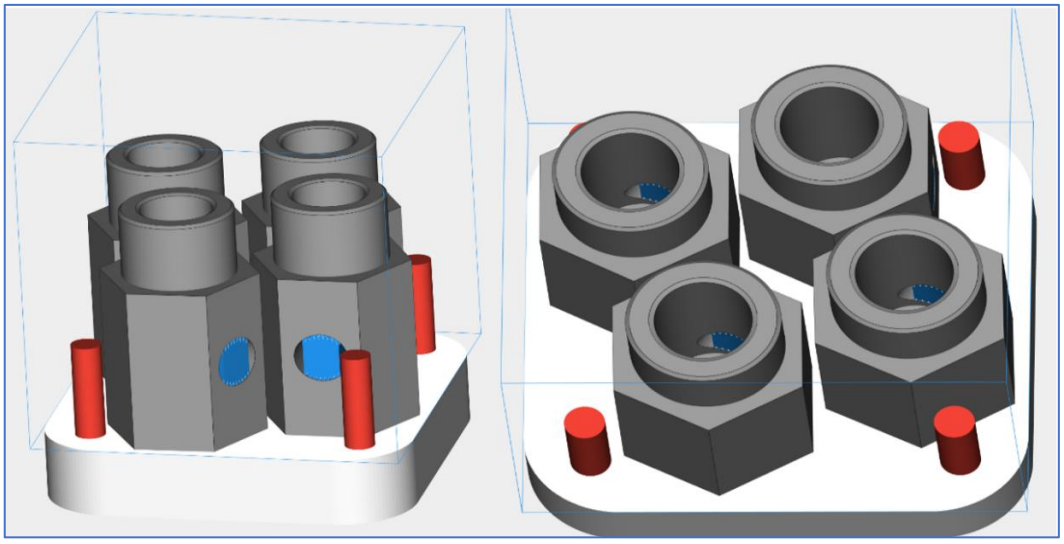

Figure 29, Manifold orientation in the build plate.

Figure 30 shows four manifolds packed very close to each other in the build plate. Nevertheless, the components are not touching each other or overhanging out of the build platform. The components are also arranged so that the re-coater does not slide over them in a "parallel" way but instead at an angle.

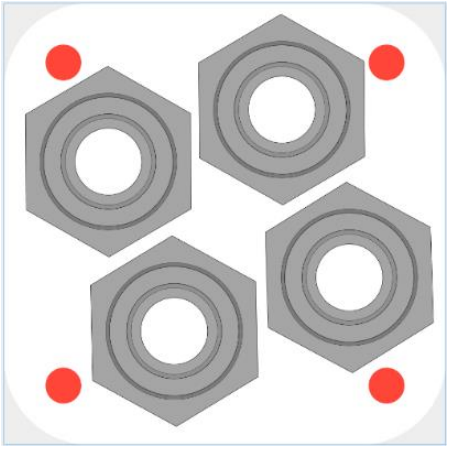

Figure 30, Manifold top view orientation in Magics Materialise software.

SLM Slicer Viewer software

Figure 31 shows the manifold component inside the software SLM slicer viewer. Image B on the right of figure 31 shows the first layer from when the printing operation starts. This simulates the actual printing profile that occurs on the SLM 125 HL machine. The first layer shows the vector lines in different colours, which means the laser will travel along those vector line directions.

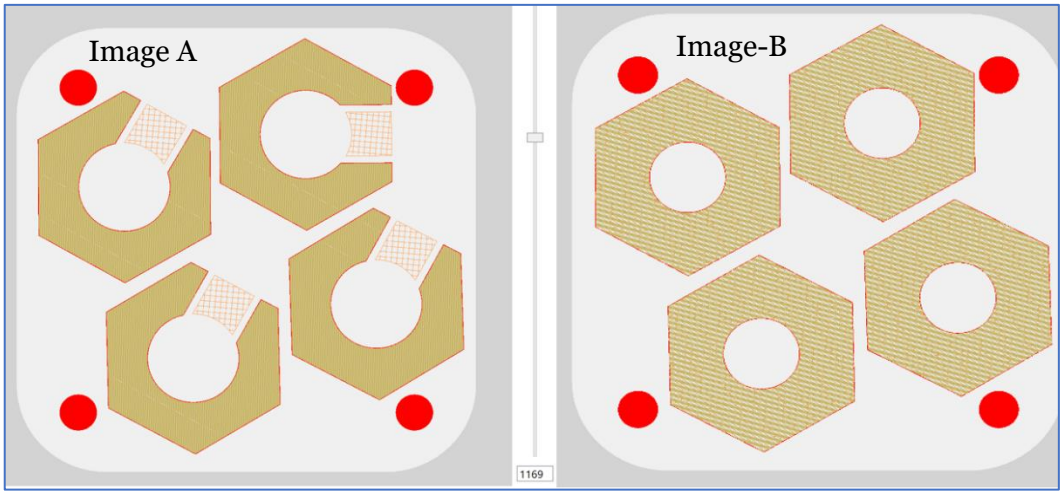

Figure 31, Manifold SLM slicer viewer.

Image A on the left side of figure 31 shows the first layer for when the printing supports have started, represented with red colour vectors. The vector also shows the direction in which the laser passes during that layer number.

In figure 31, in image A, on the right side, there is an operational bar. The software allows for dialling between each layer printed with this bar. Figure 31 shows that the printed supports during the print are located at layer number: 1169. The dial bar helps to see every layer and look for defects. Those defects could be such as a vector not changing the angle or a change in the colour of the vector completely.

It is essential to check every layer that the vectors are rotating with an angle of increments set on the printing parameters. For example, the vector rotation parameter changes every 33 degrees angle of each layer for this print job, as shown in figure 32. Figure 32 also shows the vector angle at the start of the print in the first layer as 15 degrees.

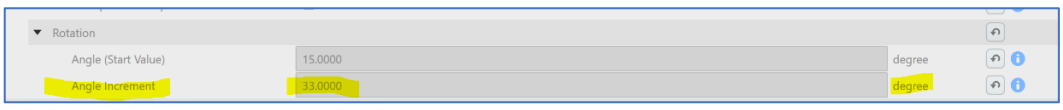

Figure 32, Printing parameters from Magics Materialise.

Figure 33 shows the final last layer from the print in pink colour with the number of the layer as 2861. The last layer also shows the vector lines that are all travelling in the same direction.

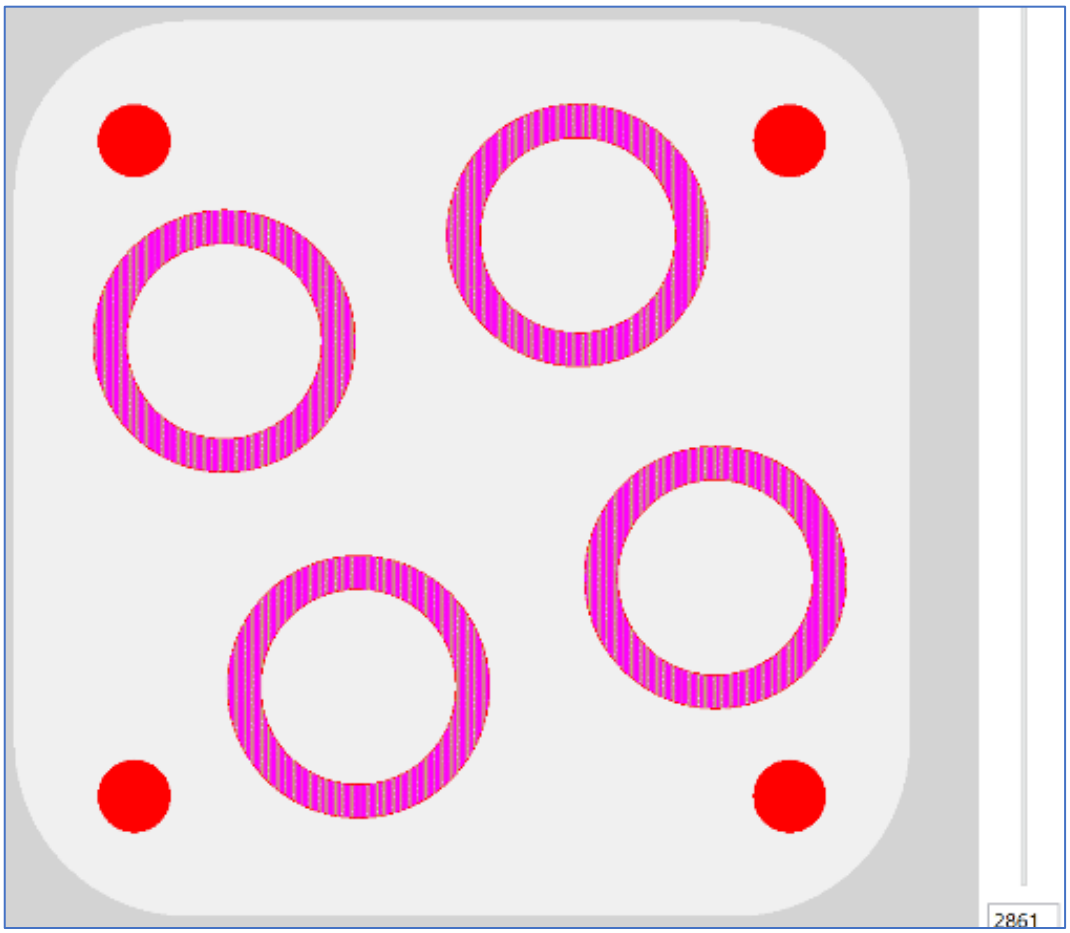

Figure 33, Manifold SLM slicer viewer top layer.

Figure 33 also shows red dots representing the bolt holes from the SLM 125 HL 3D printer. For instance, the parts cannot be placed on top of the holes so that the bolts and build plate can be removed after the print has been finalized.

Impeller build preparation

Due to the privacy and confidentiality agreements, Proventia Oy. prefers not to show the original images of the impeller. For that reason, in this chapter, the image of the impeller inside Magics Materialise software is not shown. Instead, the impeller is only shown from a top view angle from SLM slicer viewer software. The top view does not reveal any sensitive information about the genuine impeller.

The author of the thesis changed the dimensions of the impeller during the CAD model preparations. For the build preparation of the impeller, the CAD model is modified from the original sketch into a circle. This extra 1.00 mm material acts as support and has more material when the impeller is detached from the build plate with the EDM machine. The EDM machine has a wire thickness of 0.250 mm, as mentioned in chapter 2.2.2, and the build plates tend to deflect during the print due to the excessive heat generated from the lasers.

SLM Slicer Viewer software

Figure 34 shows the impeller inside the SLM slicer viewer software in the first layer. The first outside vectors are shown in red colour,

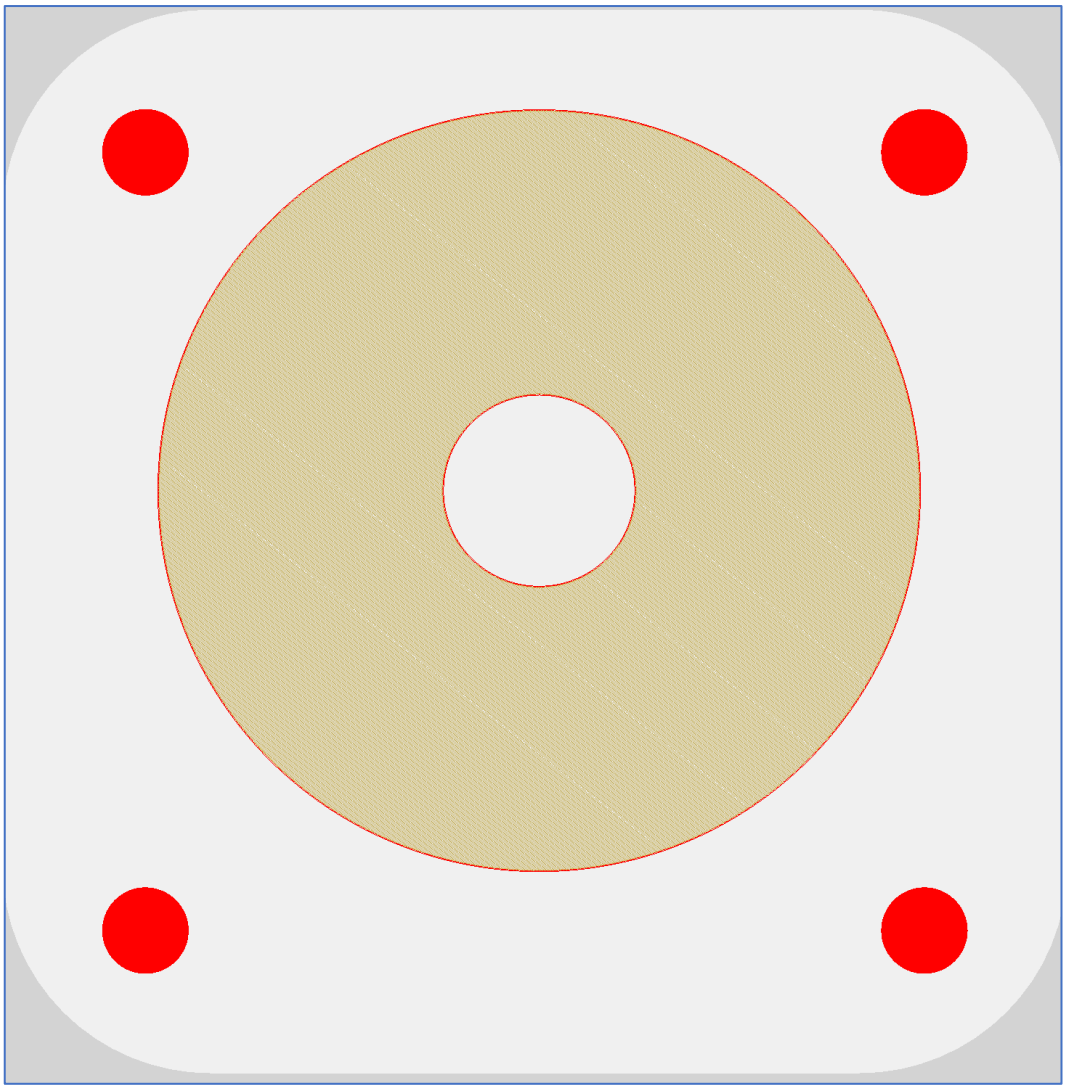

Figure 34, Top view of the impeller at the first layer in SLM slicer viewer.

Lattice pattern spur gear build preparation

Figure 35 shows the lattice pattern gear inside Magics Materialize software. Due to the diameter of the spur gear, only two were fitted in the build plate. As a result, the printing orientation was "flat", so no supports were needed.

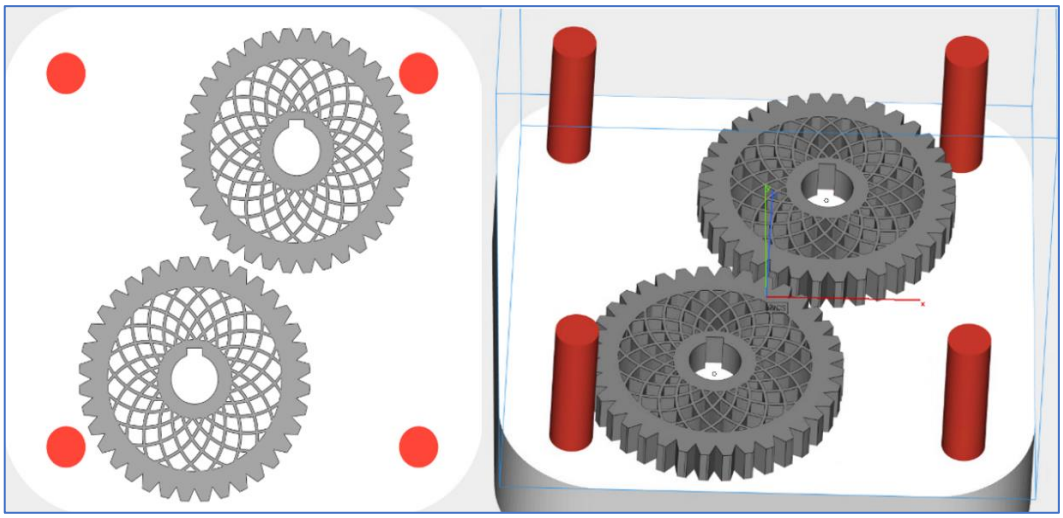

Figure 35, Lattice pattern gear in Magics Materialize.

SLM Slicer Viewer software

Figure 36 shows the lattice pattern gear in SLM slicer viewer software, the image on the right side shows the first layer printed. The image on the left shows the last final layer printed in pink. Some colour differences in the last layer are due to issues in the vector generation in the software. However, this was not a big issue since this print job was 8.5 mm in height and was sent to Oulu University for milling, removing any unevenness from the final layer.

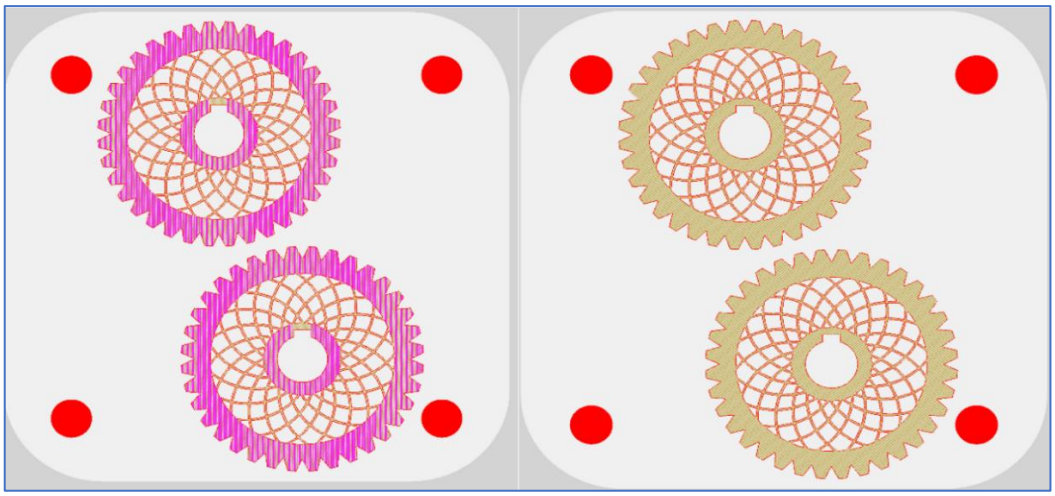

Figure 36, Lattice pattern gear in the SLM Slicer viewer.

3.3 Description of the machines

In this sub-chapter, the machines and parameters utilized for the manufacturing of the components are described.

3.3.1 SLM HL 125 powder bed fusion machine

Figure 37 shows the Selective Laser Melting System SLM 125 HL, which is 125 x 125 x 125 mm^3 build envelope. It is ideal for R&D and to manufacture small parts with a single 400 Watts laser and a build plate that heats up to 200° C. (SLM solutions, 2022)

Figure 37, SLM 125 HL from VTT's advanced manufacturing laboratory.

It is recognizable that the chosen study approach has some limitations. For instance, the SLM 125 HL is a small PBF machine, which may be regarded as a constraint due to its smaller size. On the other hand, a larger SLM machine might be more indicative of productivity and energy efficiency.

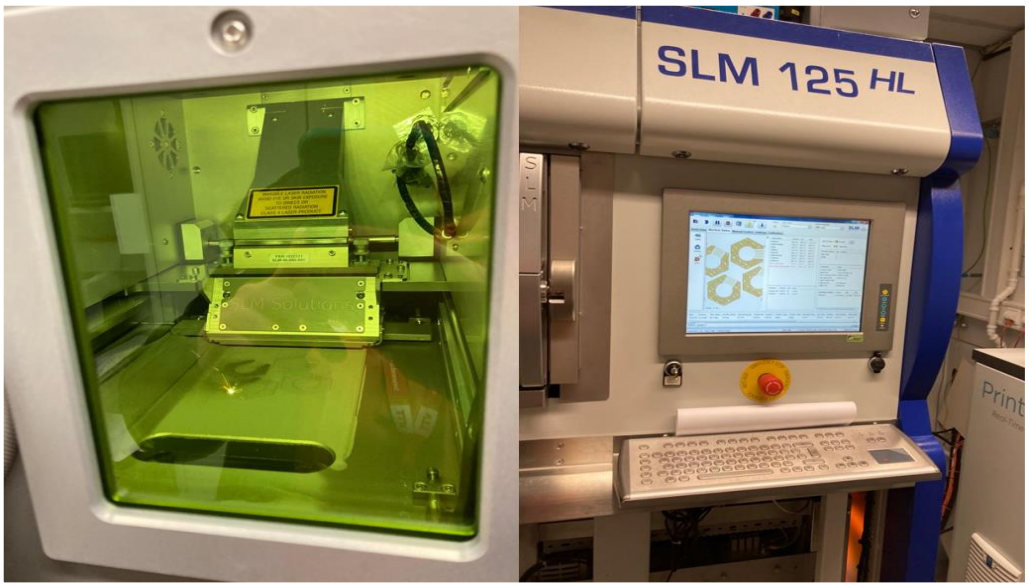

Figure 38, SLM 125 HL from VTT's Laboratory.

Figure 38 shows the left side of the chamber from the 3D printing machine from VTT. At that moment, the manifold was printed as sparks were going through the geometry inside.

SLM Parameters for the build preparations:
For this thesis work, the parameters utilized are developed and provided by SLM solutions for Stainless steel 316 L. These parameters are accessed through Magics Materialise and are divided into three main categories:

1. Machine parameters, with eight different settings
2. Build Strategy with 418 settings
3. Platform Settings with 21 settings

The main parameters that are relevant to be mentioned in the thesis are:

- For printing 30 um layer thickness:
  1. Laser power: 200 W
  2. Scanning speed: 800 mm/s
  3. Hatch distance: 0.12 mm

- For printing 50 um layer thickness
  1. Laser power: 275 W
  2. Scanning speed: 700 mm/s
  3. Hatch distance: 0.12 mm

For both layer heights, the build plate pre-heating temperature was 100 °C. The build platforms utilized were made of stainless steel 316L.

3.3.2 CNC-milling machine

The CNC-milling machine utilized to manufacture the components for this master thesis is located at Oulu University Machine shop. This is a five-axis milling machine named Mikron GF Mill E 700 U, shown in figure 39.

Figure 39, CNC-milling at Oulu University Machining Shop.

According to GF Machining Solutions (2022), the main core components from the MILL E 700 U are shown in figure 40.

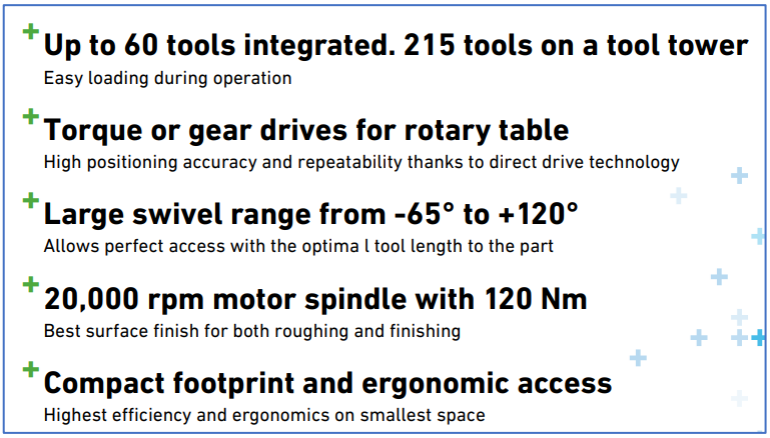

Figure 40, Core components GF milling (GF Machining Solutions, 2022).

Tools and parameters utilized for the components

For the manifold component manufactured with the five-axis CNC-milling machine, the tools and parameters are shown in table 6.

Table 6, CNC-milling tools and parameters for manufacturing the manifold.

	SEW Manifold milled Parameters		
TOOLS	Cutting speed (smm)	Feed rates (mmpm)	Spindle Speed (rpm)
End mill 12 mm	150	1591.6	3979
	169	1800	4500
	150	1273.2	3979
U drill 24.5 mm	230	400	3000
U drill 19 mm	89	175	1500
Drill 8.8	149	1300	5420
Centering drill 8 mm	200	800	8000
	100	500	8000
	201	500	8000
Plug tap G18	7	343.5	400
	12	343.5	400
Plug tap G1/2	16	250	200
Plug tap G3/4	15	250	180

For the manifold 3D printed with the SLM 125 HL and then sent to Oulu University for machining, the tools and parameters are shown in table 7.

Table 7, 3D printed manifold CNC-post-processing tools and parameters.

	SEW Manifold 3D printed CNC mill Parameters		
TOOLS	Cutting speed (smm)	Feed rates (mmpm)	Spindle Speed (rpm)
End mill 12 mm	169	1800	4500
	150	1273.2	3979
U drill 24.5 mm	230	400	3000
U drill 19 mm	89	175	1500
Drill 8.8	149	1300	5420
Centering drill 8 mm	200	800	8000
	100	500	8000
	201	500	8000
Plug tap G18	7	343.5	400
	12	343.5	400
Plug tap G1/2	16	250	200
Plug tap G3/4	15	250	180

Tables 6 and 7 show the exact amount and type of tools utilized for machining the manifold. However, one less operation is performed for the post-processing of the 3D-printed part, and the same tools are used for all the operations. For the impeller components manufactured with the CNC-milling machine, the tools and parameters are represented in table 8.

Table 8, CNC-milling tools and parameters for manufacturing the impeller.

	Proventia impeller Milled Parameters		
TOOLS	Cutting speed (smm)	Feed rates (mmpm)	Spindle Speed (rpm)
Barrel mill R2;R30;R5	157	599.64	4997
	157	600	4997
End mill 8 mm	105	835.6	4178
	105	1000	4178
	105	835	4178
	105	500	4200
	105	114.12	4178
Ball end mill D2	80	509.28	12732
	80	954.9	12732
	80	800	12732
End mill 4 mm	105	835.6	8356
	105	500	8356
	105	400	8356
Drill 5.1 mm	55	340	3433
Plug tap M6	9	250	500
Centerring drill 8 mm	50	278.46	1989
	105	500	4178

For the impeller component that has been 3D printed and then sent to the Oulu University machine shop for post-processing machining, the tools and parameters are shown in table 9.

Table 9, 3D printed impeller CNC-post-processing tools and parameters.

	Proventia Impeller 3D Printed Mill Parameters		
TOOLS	Cutting speed (smm)	Feed rates (mmpm)	Spindle Speed (rpm)
Barrel mill R2;R30;R5	157	599.64	4997
	157	600	4997
End mill 8 mm	105	1000	4178
	105	1114.12	4178
Ball end mill D2	80	954.9	12732
	80	800	12732

Tables 8 and 9 show different amounts of tools utilized; the machined part utilized seven different tools, and the 3D printed part utilized just three tools. This is because the top part of the impeller was almost manufactured perfectly with the SLM, and only a finished mill operation was needed to achieve a good surface quality. After that, the rest of the operation was performed to make the under shape.

Table 10 shows the tools and parameters from the solid spur gear CNC-machined.

Table 10, CNC-mill parameters and tools for manufacturing the solid gear.

	Solid Spur Gear Milled Parameters		
TOOLS	Cutting speed (smm)	Feed rates (mmpm)	Spindle Speed (rpm)
End mill 8 mm	100	400	3979
Module mill D21.7	100	60	1467

Table 10 shows that two different tools have been utilized for the CNC-milling of the solid spur gear.

Table 11, 3D printed lattice gear CNC-post-processing tools and parameters.

	Lattice Pattern Gear Milled Parameters		
TOOLS	Cutting speed (smm)	Feed rates (mmpm)	Spindle Speed (rpm)
End mill 8 mm	100	400	3979
Module mill D21.7	100	60	1467

Table 11 shows the same number of tools utilized and the same number of operations and values for all the parameters.

3.3.3 CNC-lathe machine

The CNC-lathe utilized at Oulu University is an Okuma LB 3000 EX II, shown in figure 41.

Figure 41, CNC-Lathe machine from Oulu University.

Table 12 shows the machine parameters and tool names utilised for the manufacturing of the manifold with CNC-lathe. There were nine different tools utilized for this machining and 12 different operations

Table 12, Manifold CNC-lathe machine parameter.

SEW manifold CNC lathe machined parameters		
Tools:	**Cutting speed (m/min):**	**Feed rates (mm/rev):**
External turning tool	140 180	0.2 0.2
U drill 19 mm	120 0.06	0.15 0.15
Plug tap G1/2	15	1.814
Plug tap G3/4	15	1.814
Drill 8.8 mm	150	0.1
Plug tap G18	15	0.907
Drill 19 mm	30	0.2
Second Plug tap G1/2	15	1.814
Parting off turning tool	80	0.08

3.3.4 EDM electrical discharge machining

The wire-cutting machine or EDM utilized in this thesis was the Charmilles Robofil 440 from the Aalto University machining shop. This EDM utilizes a wire for cutting, which is 0.250 millimetres in diameter. Figure 42 shows the EDM wire-cutting machine utilised in this study.

Figure 42, EDM wire cutting machine from Aalto University machine shop.

Figure 43, Wire from EDM machine at Aalto University.

Figure 43 shows the small thickness of the wire, and this method allowed the components to be cut out of the build plate without wasting much material. The EDM utilizes six meters per minute of brass wire. Currently, the wire costs around 200 € per 20 km, and it weighs 8 kg.

3.3.5 Energy meters

Two different measurement devices have been utilized to measure the energy of the components during the manufacturing phase. One device was installed in the CNC-mill machine and CNC-lathe machine at Oulu University. The other device was for the 3D printer SLM 125 HL at VTT's laboratory and the EDM wire-cutting machine at the Aalto University machining shop.

CNC-machines

The CNC-machine utilizes a Shelly EM energy meter installed outside both CNC-machines, shown in figure 44.

Figure 44, Shelly EM energy meter installed in the CNC-lathe machine at Oulu University.

Shelly EM stated to Oulu University that the measurement unit error percentage is 1% for this device. This device measures three phases of electricity and sends it to application software to extract the data. It utilizes Wi-Fi to monitor the energy consumption shown in figure 45. It can monitor any electrical device and control heavy-load machines. (Shelly EM, 2022) Shelly EM measures the energy intake into the machine per minute and second. For this study, the data per second was utilized.

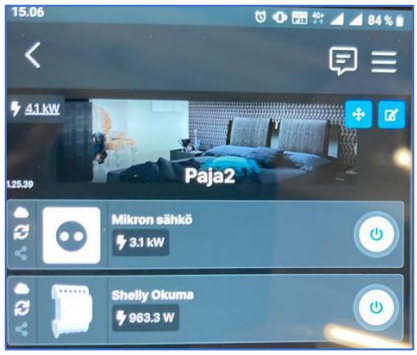

Figure 45, Shelly monitoring unit from Oulu University.

SLM 125 HL and EDM wire cutting

The SLM machine and the EDM wire cutting utilized an ABB energy meter. The name of the model is "B23_212_100" (ABB, 2013). This energy meter can measure one and three phases in kWh. According to ABB, p.73 (2013), "The accuracy or measurement error is usually tiny, typically 0 to 2 %". The measurement interval for the ABB meter is 1 second.

Figure 46, ABB energy meter at VTT laboratory.

Figure 46 shows the energy meter installed at the VTT laboratory next to the SLM 125 HL to measure the 3D prints. This same measurement device was taken to the Aalto University machine shop in Otaniemi Espoo to measure the energy consumed to detach the components from the build plate.

3.4 Inventory for LCI

The LCI inventory exhibits the type of data collected and the unit values. For the primary data collected from the CNC-machining and the SLM 3D printing, the electricity is presented in kilo Watts hour (kWh).

For the material utilized for the solid feedstock and metal powder, the unit utilized for the weight of the part and amount of waste is in Kilograms (kg).

For the argon gas consumption, the unit measured in the pressure drop in Bar. Therefore, the argon consumption amount is presented in kilograms of argon gas (kg/argon),

3.4.1 Argon gas measurement

The argon gas was procured from Woikoski Oy in a bottle of 50 litres with a pressure of 200 bar (Woikoski Oy., 2022). The pressure readings were from a 50 mm diameter pressure gauge Wika 111.11.050 (accuracy level CL 2.5) installed in regulator AGA D204-50 C B-R.

In order to measure the amount of argon gas consumed every time a build operation passes, two approaches can be taken. One approach is utilizing Boyle's law, and another approach can be the "Ideal gas law".

However, given the nature of the data gathered, the most reliable method is applying the law of ideal gases. For this to happen, the pressure difference before and after the print is ignored for the gas compressibility factor because argon gas can be approximated to a value of $\boldsymbol{z = 1.}$ (Gas Encyclopaedia Air Liquide, 2022)

The ideal gas law is given as follows:

$$\boldsymbol{pV = n\,R\,T} \qquad \text{Eq. 1 (Seppänen \& Jansson, 2006)}$$

Where p is the pressure in bar, V is the volume in m^3, n is the number of moles in mol, R is the universal gas constant of $0.08314\ L\ bar\ mol^{-1}\ K^{-1}$, T is the temperature in K. (Seppänen & Jansson, 2006)

Since the volume V is fixed at a constant $50\ L$ (the size of the argon gas bottle), R is constant. The temperature T can also be considered constant (assumed room temperature $T = 293\ K$).

Hence, the measurement will be small enough to enable a linear relationship between the pressure p and the number of moles n can be calculated.

After levelling the measurement and before using the first $p_1$and the measurement after the use as p_2, is as follows:

$$p_1 V = n_1 RT$$

$$p_2 V = n_2 RT$$

$$(p_1 - p_2)V = (n_1 - n_2)RT$$

$$(n_1 - n_2) = \frac{(p_1 - p_2)V}{RT}$$

Thus, the number of moles will be linearly dependent on the difference in the pressure measured. So then, the number of moles can be related to the mass of gas used as:

$$m_{Ar} = 39.948\ g/mol \quad \text{(Boudreaux, 2022)}$$

$$M_{Ar} = m_{Ar} \cdot n_{Ar}$$

Thus, a direct relationship between the difference in pressure in the bottle and the mass of the gas spent can be determined. According to the measurements, that relationship can be established as follows:

$$(n_1 - n_2) = \frac{(200\ bar - 186\ bar) \cdot 50\ L}{0.08314\ L\ bar\ mol^{-1}\ K^{-1} \cdot 293\ K} = 28.736\ mol$$

$$M_{Ar} = 39.948 \frac{g}{mol} \cdot 28.736\ mol = 1.1479\ kg$$

Therefore, it was calculated that if $1.1479\ kg$ of gas were spent when the pressure dropped $14\ bar$, there is a consumption $C = 0.082\ kg/bar$.

This leads to a final calculation of $M_{Ar_{spent}} = (p_1 - p_2)C$.

This means, for example, that if a process produces a drop of $5\ bar$ in the pressure of the bottle, the process consumed a total of $M_{Ar} = (5\ bar) \cdot 0.082\ kg/bar = 0.41\ kg$.

Finally, when the same rule is utilized, it can be established that a full bottle contains $16.4\ kg$ of argon gas.

This method and formulas were inserted in Microsoft Excel for calculating the argon gas consumption during the filling and operation of the SLM 125 HL and for each print builds.

For the filling of the chamber of the SLM 125 HL with argon gas, the same value has been given to all the prints; 1.147 kg. This amount was calculated the same way as the 3D printing and added to each build during the 3D printing operation.

3.4.2 Metals raw materials

For the SLM 3D printer, the metal powder utilized was Högänäs 316L 20-53 µm, and its chemical composition is represented in table 13.

Table 13, SS 316 L powder chemical composition (Höganäs, 2022).

Fe (%)	Ni (%)	Cr (%)	Mn (%)	Si (%)	Mo (%)	C (%)
Bla	12.0-14.0	16.0-18.0	Max 0.2	0.5-1.0	2.0-3.0	Max 0.03

According to the material data sheet, stainless steel 316 L has a density of 8000 kg/m^3 at 20°C (Thyssenkrupp Materials, 2022).

The manifold part was manufactured from hexagonal steel in the CNC-mill and lathe machine, and the material code is: "11SMn30+C h11 AV46 AUTOMATIC". The density for 11SMn30 is 7800 kg/m^3 (Steel Navigator, 2022). For the impeller and the gear solid, the parts were manufactured from a solid round bar made of Stainless steel 316 L

Material Waste Calculations

For all the CNC-machining operations, the plank of feedstock material was weighed before the start. Then, when the component was completed, it was weighed again. The chip waste was found by calculating the difference between the plank material weight from the component weight.

For the 3D printed components, the waste was calculated by:

- Weigh the filter waste
- Sieving the unused powder
- Weigh the sieved waste
- Weighing the build platforms empty
- Weighing the platform with the parts
- Subtract the difference weight from the platform with the parts and empty platform to find the weight of the part.

For all the EDM wire cutting, the waste measurement was calculated by:

- Weigh the parts after being cut off the platform
- Weigh the platform after wire cutting
- Subtract the weight of the part made by SLM from the EDM part
- Subtracting the weight of the empty platform from the EDM platform

3.4.3 Measurements of energy consumption

CNC-machining

For the CNC-lathe and mill machine, an extra amount of energy has been added to the energy during the operational machining. This extra energy was allocated when the machine was on standby. Also, it was allocated for the energy consumed between the operations and during the warming up of the machine. Oulu University has given the energy values for the stand-by and warm-up of both machines.

For the CNC-Lathe machine, the energy consumed was:

- The standby was 0.3 kWh for 8 hours per day from Monday until Friday.
- The warmup was 0.0468 kWh, which took 4 minutes and 5 seconds.

For the CNC-mill machine, the energy consumed was:

- The standby was 3.2 kWh for 8 hours per day from Monday until Friday.
- The warm-up was 0.0319 kWh, and it took 18 minutes and 10 seconds.

Warm up energy

For the standby of the CNC-machine, the values given by Oulu University were divided in two. If 3.2 kWh and 0.3 kWh is the value of the amount of energy for one hour divided by two means, it would be during the time laps of 30 minutes instead of one hour. If the machine operator would take 15 minutes to prepare the machine before starting the operation and another 15 minutes to clear the new part out of the machine and other tasks, then a total of 30 minutes of standby was given to each machine. This value was added to the final amount of energy consumed during the manufacturing each part. The warmup of the CNC-machine was calculated after gathering the information on the time elapsed to produce each part. Since in this experiment only one part was created, the amount of time each part took to manufacture was divided into eight hours. This value would assume how many of these parts can be manufactured during eight hours because the machine only warms up once daily, usually in the morning. For that reason, dividing the warmup of the CNC-mill (0.0319 kWh) into a possible number of parts that can be produced in one day. This calculation was concluded individually for each component for the CNC-mill and CNC-lathe because of the different manufacturing times per part.

SLM machine

The standby and cool-down energy consumption time for the SLM machine were measured directly from the ABB energy meter. The standby for one hour was calculated to be 0.92 kWh. For the standby and cool-down time, the total amount of 30 minutes has been given, and 0.463 kWh was added to all the builds.

3.4.4 LCI scenario modelling-process flow chart

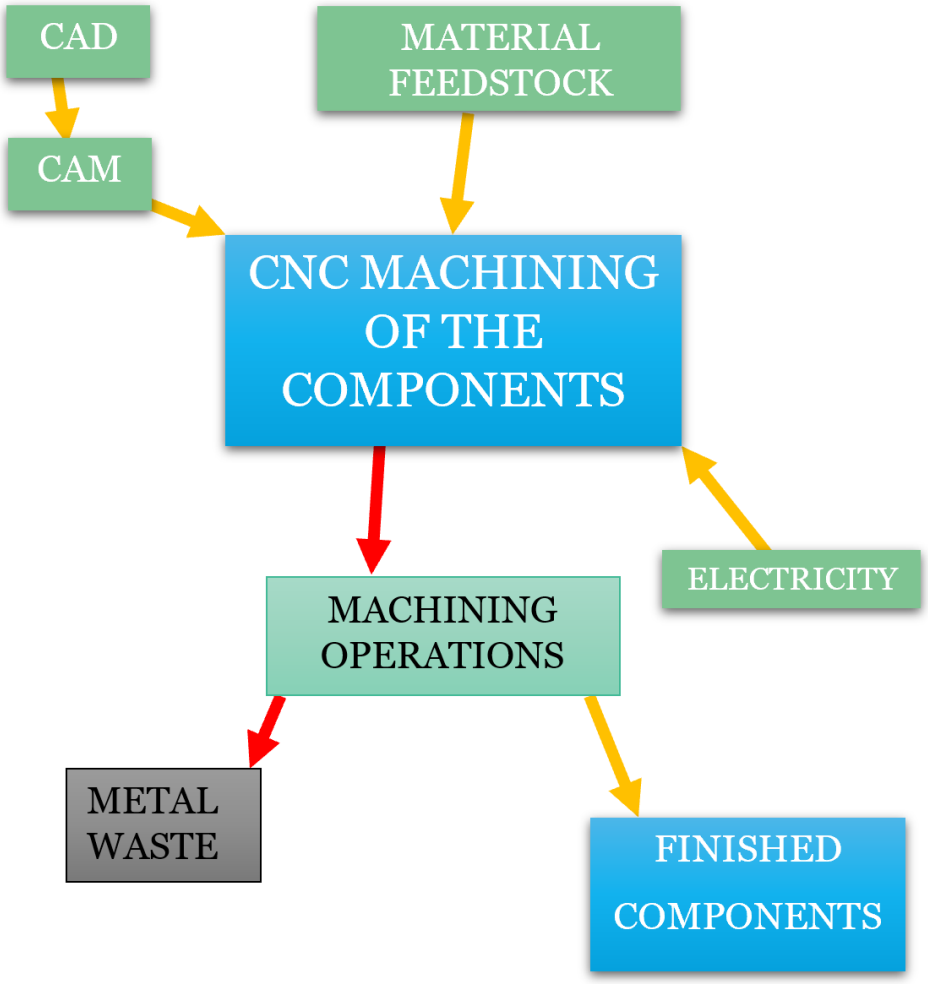

Figure 47, CNC-machining of the component process flow chart.

Figure 47 shows that in yellow are the arrows for input values, and in red are the arrows for the output and waste. This process flow chart is missing many inputs of the CNC-machining operations, but those inputs are not considered in this thesis study. For example, utilization of water and cutting fluid, tool wear or transportation.

PBF input-output process flow chart for one component

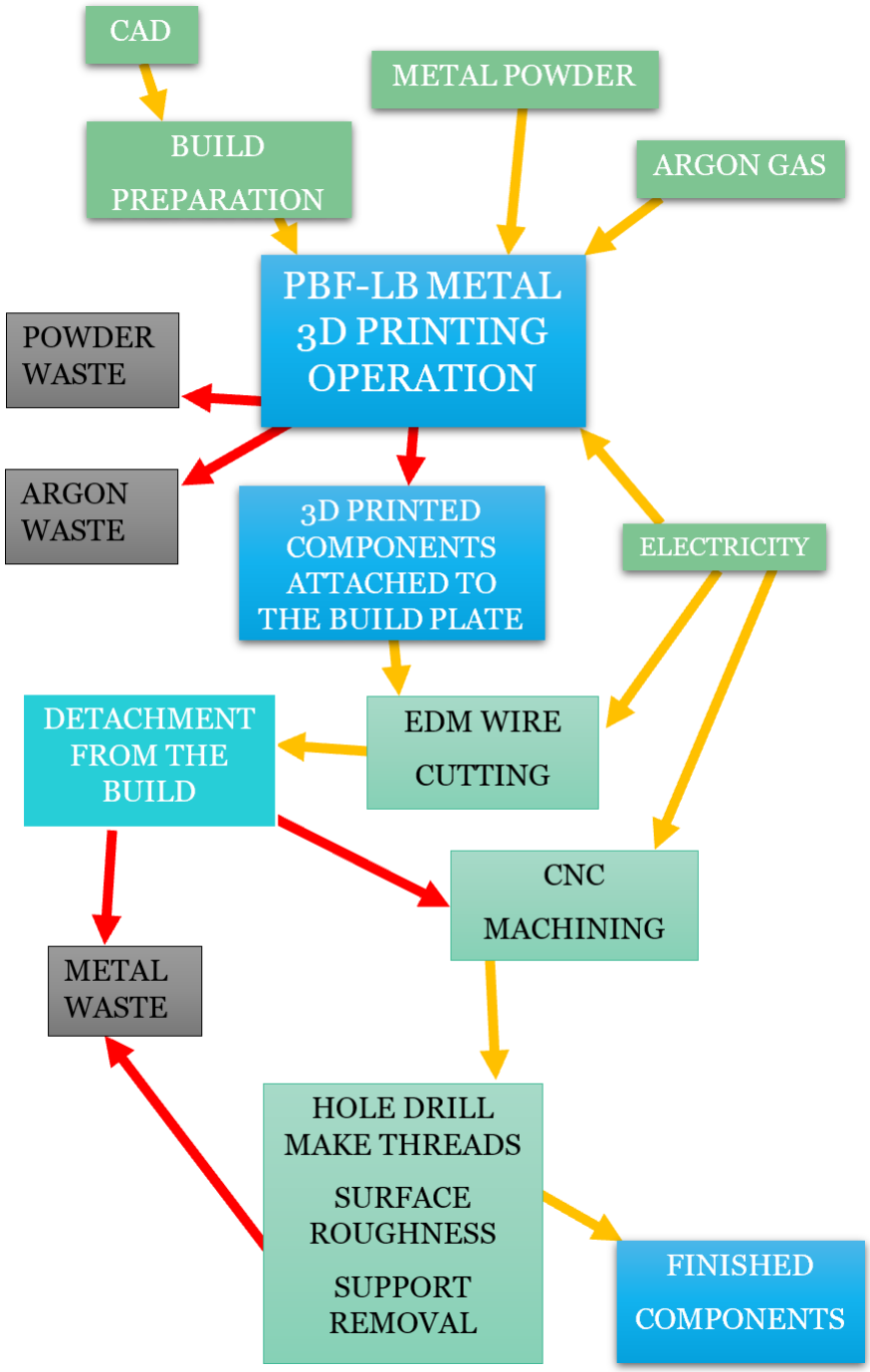

Figure 48, Metal 3D printing PBF of the components process flow chart.

Figure 48 shows in yellow colour the arrows for input values and in red colour the arrows for the output and waste. There is no auxiliary equipment in the chart as it is not part of the scope of this thesis. This flow chart represents the start of the CAD model and the process taken in this thesis study, from PBF to EDM to CNC machining for post-processing.

4 Results & analysis

The energy, material and argon gas consumption of the components manufactured are presented in this chapter. Also, the warm-up and stand-by energy values are presented. For the 3D-printed parts, the results are presented in a sequence. Starting with the 3D printing in the SLM 125 HL, continuing from when parts were separated from the build plate with EDM. Finally, the parts were CNC-machined for post-processing to remove the extra material and converted into functional parts.

CNC-machining warm-up time

Table 14, Machined parts that could be produced in one working day.

Component	Machine Time (hours)	N º parts/8hs	Warm-up (Wh)
Manifold in Mill	0.183	43.636	7.324
Impeller	1.169	6.843	46.701
Gears	0.478	16.736	19.096
Manifold in Lathe	0.14	57.142	0.819

Table 14 shows the number of parts that could be manufactured per day for each component in the yellow column. This is used to allocate the warm-up energy, as described in chapter 3.4.3. The energy is presented in Watts hour.

4.1 Manifold

Manifold manufactured with CNC-Mill machined only

Figure 49, Manifold manufactured with CNC-Mill machine.

Figure 49 shows the manifold produced with the CNC-mill machine. The manufacturing consumed 0.702 kWh of energy, and the operation time was 10.78 minutes. The plank material weight was 1.270 kg, the weight of the finished part was 0.720 kg, and the waste material was 0.550 kg.

Manifold manufactured with CNC-Lathe machined only

Figure 50, Manifold manufactured with CNC-lathe machine.

Figure 50 shows the manifold component made by the CNC-lathe only. The manufacturing consumed 0.456 kWh of energy during 8.42 minutes of operational time. The plank material was 1.275 kg, the finished part weight was 0.720 kg, and the waste material was 0.555 kg.

PBF-SLM 3D printed four-manifolds in one build

Figure 51, Manifold in the SLM 125 HL, four parts in one build.

Figure 51 shows four manifold 3D printed in one build plate. This process consumed 112 kWh during 65.2 hours. The consumption of metal powder was 4.708 kg, and the combined weight of the 3D-printed four parts was 3.182 kg. The powder waste from this process was 1.526 kg. The argon gas consumption only during 3D printing for this build was 6.055 kg.

EDM separation of the components from the build plate

Figure 52, Manifold detached from the build plate with EDM process,

Figure 52 shows the manifold cut out of the build plate with the wire-cutting machine. This process consumed 9.88 kWh during 131 minutes of operation. The weight of the finished four parts was 3.160 kg, and the waste material was 0.021 kg. Hence each individual manifold part weight was 0.790 kg.

The final machined part after post-processing

Figure 53, SLM 3D printed manifold after the CNC-mill post-processing.

Figure 53 shows the manifold after machining with a CNC-lathe for thread making and removing extra material from the bottom to meet the dimension shown in the 2D drawing. The energy measurement was performed for every single manifold. For every single manifold operation, the energy consumption was 0.772 kWh and took 9.58 minutes. Each manifold plank was 0.790 kg before this operation, the finished part weight 0.730 kg, and the waste was 0.060 kg.

4.2 Impeller

The images after 3D printing and machining cannot be shown for the impeller, as explained in chapter 3.1.2.: “Due to confidentiality and IPR protection, Proventia has asked VTT not to show any 2D drawings, CAD models, or images of the actual component”.

CNC-machine part only

For the manufacturing of the impeller with the CNC-mill machine, the energy consumed was 5.209 kWh during 70.13 minutes of operation. The plank material weight was 1.01 kg, the finished part weight was 0.270 kg, and the waste material was 0.740 kg.

SLM-PBF 3D printed

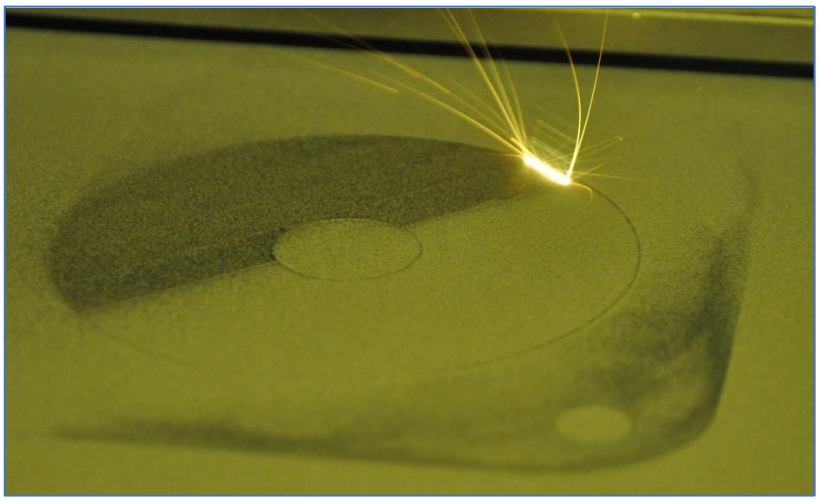

Figure 54, Impeller inside the SLM 125 HL chamber.

Figure 54 shows the impeller inside the print chamber of the SLM machine during the first layers. There are two different energy, material, and gas consumption for this part, as mentioned in chapter 3.1.2. One part was printed with a layer height of 30 µm, and the other was printed with a layer height of 50 µm.

For the 30 µm, the energy consumption was 13.87 kWh, and the operation took 6.917 hours. The consumption of metal powder was 0.595 kg, the finished part weight was 0.388 kg, and the waste powder was 0.206 kg. The argon gas utilised for this 3D printing build operation was 0.574 kg.

For the 50 µm layer height impeller, the energy consumption was 10.28 kWh for 5.1 hours. The input of metal powder was 0.537 kg, the part finished 0.381 kg and the waste powder 0.156 kg. The argon gas utilised for this build was 0.410 kg.

Impeller PBF-3D printed EDM post-process

For the impeller, the separation of the component out of the build plate with the EDM process, the energy consumption was different for the 30 and 50 µm. The consumption for the 30 µm impeller was 7.75 kWh during 100 minutes of operation, the weight of the finished part was 0.358 kg, and the waste material was 0.031 kg. The consumption for the 50 µm was 7.27 kWh for 103 minutes, the weight of the part was 0.349 kg the waste material was 0.030 kg.

Impeller final PBF post-process with CNC mill

The energy consumed for this process is assumed to be the same for both impellers produced with the 50 µm and the 30 µm layer height. As a result, just one component was machined. The energy consumed for the final machining of the impeller was 1.999 kWh during 25.17 minutes of operation. The part plank material weight was 0.358 kg, the finished part weight was 0.265 kg, and the waste was 0.093 kg.

4.3 Spur gear

Solid gear CNC-machined only

Figure 55, Solid Spur gear CNC-mill machine.

Figure 55 shows the solid spur gear manufactured with the CNC-mill machine. This operation consumed 2.177 kWh during 28.68 minutes. The plank material weight was 0.175 kg, the part finished weight was 0.150 kg, and the material waste was 0.025 kg.

3D printed Lattice Pattern Spur Gear

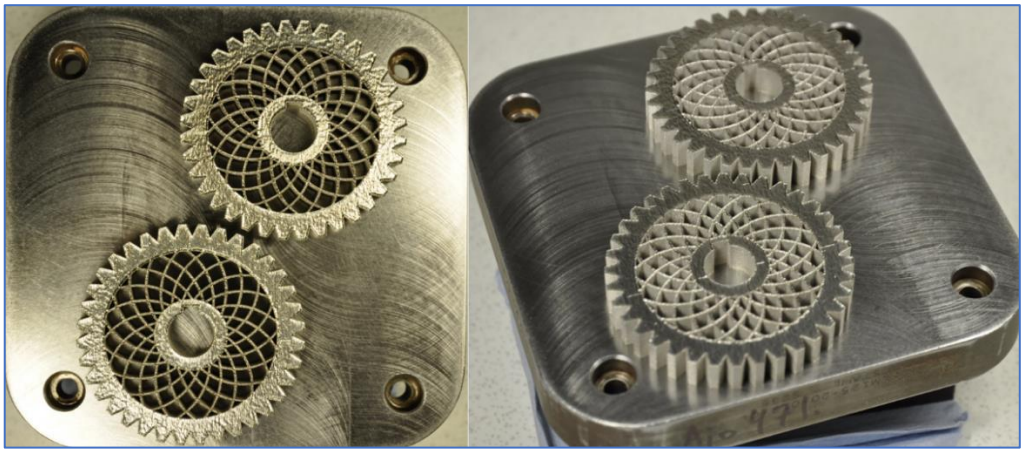

Figure 56, Lattice pattern gear printed with the SLM machine.

Figure 56 shows two lattice gear 3D printed in one build in the SLM machine. The energy consumption for this operation was 11.64 kWh during 6.05 hours. The metal powder consumption was 0.342 kg, the two finished part weight was 0.203 kg, and the waste material was 0.138 kg. The argon gas consumed during this build was 0.820 kg.

EDM separation

Figure 57, Lattice pattern gear detached from the build platform with EDM.

Figure 57 shows the lattice pattern gear when cut off from the build plate with the wire cutting EDM. The energy consumed for this process was 4.97 kWh during 80 minutes. The weight of the two finished gears was 0.192 kg, and the waste from this operation was 0.011 kg.

Final machined part

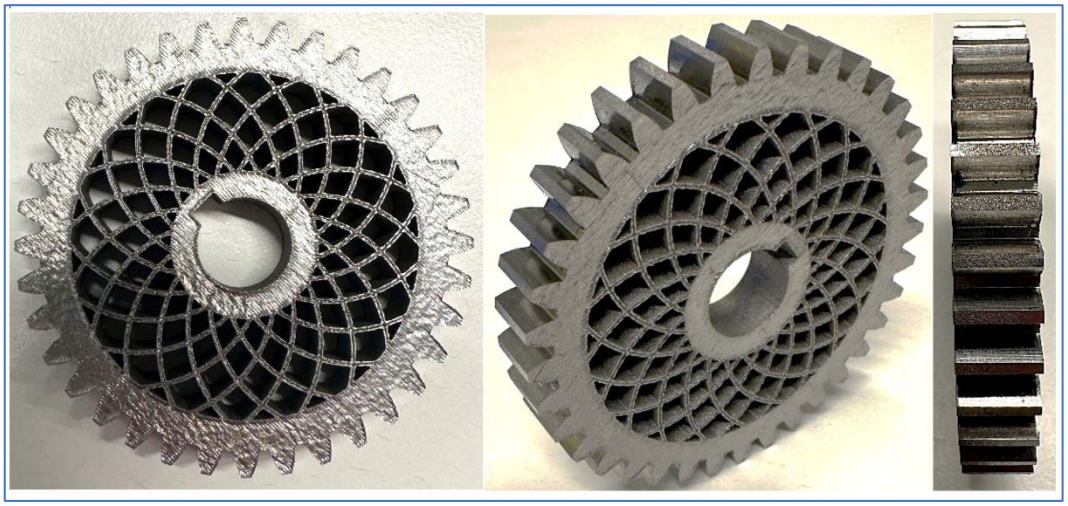

Figure 58, Lattice pattern gear 3D printed, final machining.

Figure 58 shows the 3D-printed lattice pattern spur gear after being machined at Oulu University to remove the extra material from the tooth and width to meet final dimensions and tolerances. This machining operation was performed with the CNC-mill machine and consumed 1.079 kWh during 14.28 minutes. The gear weight after separation with the EDM was 0.096 kg. After the final machining, the part finished weight was 0.090 kg, and the waste material was 0.006 kg.

4.4 Table results from CNC and SLM

CNC-Machining Energy

The total energy consumed for each component manufactured with CNC-machining is a result of adding the following: standby, warm up and operational energies. The total sum is presented in table 15 in the last column on the right. Table 15 shows the manifold twice because it was machined with a CNC-lathe and CNC-mill machine. Table 15 is the concluding energy from the complete manufacturing of each component with CNC-machining.

Table 15, CNC-machined sum of total energy consumed for manufacturing.

CNC MACHINED		STAND-BY	WARM UP	COOL DOWN	OPERATION	TOTAL SUM
Components:	Method:	kWh	kWh	kWh	kWh	kWh
SEW Manifold	LATHE	0.15	0.000819	no need	0.456	**0.606**
SEW Manifold	MILL	1.6	0.007	no need	0.702	**2.309**
PROVENTIA Impeller	MILL	1.6	0.047	no need	5.209	**6.856**
SOLID GEAR	MILL	1.6	0.019	no need	2.177	**3.796**

CNC-Machining waste

The waste material from each component that has been manufactured only with CNC-machining is represented in table 16. The manifold manufactured with the lathe has 0.005 kg more waste material than the mill machine due to the slightly larger plank material weight.

Table 16, Waste material from all the components made on CNC-machine.

Components:	Method:	Plank (kg)	Part finished (kg)	Waste (kg)	Material Type:
SEW Manifold	LATHE	1.275	0.72	0.555	11SMn30+C
SEW Manifold	MILL	1.27	0.72	0.55	11SMn30+C
PROVENTIA Impeller	MILL	1.01	0.27	0.74	SS316 L
SOLID GEAR	MILL	0.175	0.15	0.025	SS316 L

4.4.1 SLM metal 3D printed results

SLM 3D printing energy

Table 17, Sum of the total energy per build made in the SLM machine.

SLM 3D PRINTED	Method:	STAND-BY kWh	WARM UP kWh	COOL DOWN kWh	OPERATION kWh	TOTAL SUM kWh
PROVENTIA Impeller 30 µm	SLM	0.463	no need	0.463	13.87	**14.796**
PROVENTIA Impeller 50 µm	SLM	0.463	no need	0.463	10.28	**11.206**
4X SEW Manifold 30 µm	SLM	0.463	no need	0.463	112	**112.926**
2X Lattice Pattern Gear 30 µm	SLM	0.463	no need	0.463	11.64	**12.566**

Table 17 shows the total energy consumed per each build manufactured in the SLM machine. The machine is turned on, consuming standby energy while filling the argon gas inside the chamber. Also, for this study with SS316L, the build plate is warming to 200 °C during this time. The cooldown energy is allocated to the parts cooling down after the print finalizes. The total adds standby, cool down, and operational energy for each part.

EDM wire-cutting energy

Table 18, Sum of the total energy for the separation of the builds with EDM.

Detachment from Build plate	Method:	STAND-BY kWh	WARM UP kWh	COOL DOWN kWh	OPERATION kWh	TOTAL SUM kWh
PROVENTIA 30 µm	EDM	2.366	no need	no need	7.75	**10.116**
PROVENTIA 50 µm	EDM	2.366	no need	no need	7.27	**9.636**
4X SEW Manifold 30 µm	EDM	2.366	no need	no need	9.88	**12.246**
2X Lattice Pattern Gear 30 µm	EDM	2.366	no need	no need	4.97	**7.336**

Table 18 shows the total energy consumed by the EDM machine separating the build plate of the components. No warmup energy is needed in this process.

SLM post-processing with CNC-mill machine

Table 19, Total energy of the 3D components CNC-mill post process.

CNC Finishing operation	Method:	STAND-BY kWh	WARM UP kWh	COOL DOWN kWh	OPERATION kWh	TOTAL SUM kWh
PROVENTIA Impeller	MILL	1.6	0.047	no need	1.999	**3.646**
1X SEW Manifold 30 µm	MILL	1.6	0.007	no need	0.772	**2.379**
1X Lattice Pattern Gear 30 µm	MILL	1.6	0.019	no need	1.079	**2.698**

Table 19 shows the sum of all energy consumed for the 3D printed component for the CNC-post-processing operations. These operations were after the components had been separated from the build plate. For the CNC-machining, there is no cool-down required, just standby, warmup and operational energy.

Total energy utilized to manufacture the components with SLM

Table 20, Sum of the total energy from SLM, EDM and CNC-post-process.

Components:	TOTAL SLM kWh	TOTAL EDM kWh	TOTAL CNC kWh	TOTAL SUM kWh
PROVENTIA Impeller 30 µm	14.796	10.116	3.646	**28.558**
PROVENTIA Impeller 50 µm	11.206	9.636	3.646	**24.488**
1X SEW Manifold 30 µm	28.232	3.062	2.379	**33.672**
1X Lattice Pattern Gear 30 µm	6.283	3.668	2.698	**12.649**

Table 20 shows the summation between the total SLM energy consumed, the EDM total energy, and the CNC total energy. These three processes were needed to manufacture the components with the SLM machine.

SLM materials waste

Table 21, Total waste of material for each 3D printed component.

CALCULATION FOR THE TOTAL MATERIAL WASTE (kg)				
Components:	**SLM**	**EDM**	**CNC**	**TOTAL (kg)**
PROVENTIA Impeller 30 µm	0.207	0.031	0.094	**0.332**
PROVENTIA Impeller 50 µm	0.157	0.030	0.094	**0.280**
1X SEW Manifold 30 µm	0.381	0.021	0.060	**0.463**
1X Lattice Pattern Gear 30 µm	0.069	0.006	0.006	**0.081**

Table 21 shows the calculated waste for each component 3D printed with the SLM machine. Before and after each process, the part was weighed to calculate the waste. The total waste was summed starting from the SLM (3D printing of the component), plus the EDM (detachment from the build plate), plus the CNC (final post-process to create functional parts).

Table 22, Total consumption of argon gas during 3D printing with SLM.

	ARGON GAS TOTAL UTILIZATION		
Components:	**3D printing (Kg)**	**Filling SLM (kg)**	**Total (kg)**
PROVENTIA Impeller 30 µm	0.574	1.148	1.722
PROVENTIA Impeller 50 µm	0.410	1.148	1.558
1X SEW Manifold 30 µm	1.514	0.287	1.801
1X Lattice Pattern Gear 30 µm	0.410	0.574	0.984
4X SEW Manifold 30 µm	6.055	1.148	7.203
2X Lattice Pattern Gear 30 µm	0.820	1.148	1.968

Table 22 shows the total argon gas consumption from the components manufactured with the SLM machine. For the manifold and the lattice gear, the amount of argon during 3D printing and filling of the SLM machine chamber has been divided with the number of parts in each build. For the manifold, the argon gas was divided into four because it had four parts in the build plate during the print. For the lattice gear, the argon gas was divided in two because it had two gears in one build plate during the operation of 3D printing.

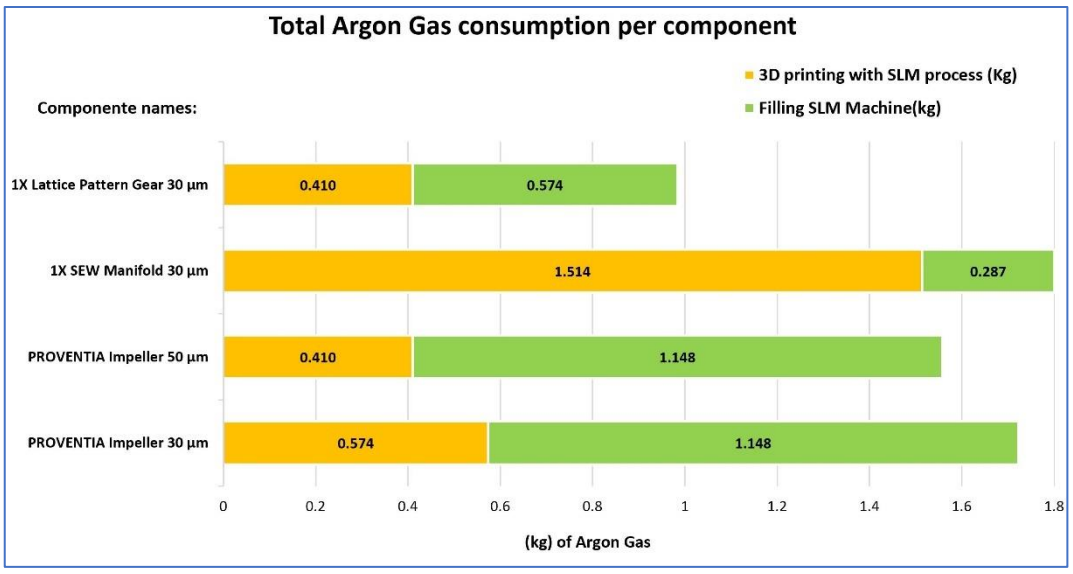

Figure 59, Total argon consumption graph in two stages.

Figure 59 shows the total argon consumption in this study and four builds manufactured with SLM 125 HL machine. The total consumption is comprised of two parts, filling the chamber of the machine before printing and during the 3D printing of the parts. It is highly noticeable that the manifold component has the highest argon consumption during printing and the lowest during machine filling. This is because these components took 65.2 hours to be 3D printed, with four-manifolds in one build. Hence, the argon gas flowed through the chamber all that time, but that time was divided into four to get 1.514 kg of argon gas. The smallest consumption during 3D printing was for the lattice gear and the impeller with 50 µm layer height, with only 0.41 kg.

4.5 Comparison results (graphs)

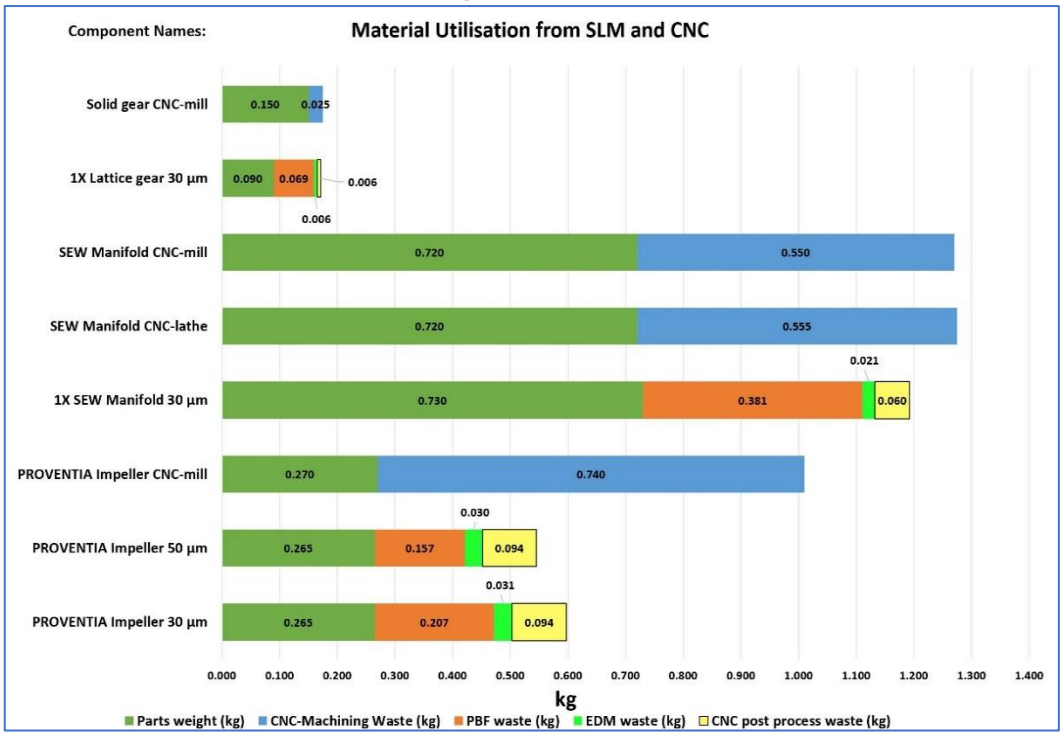

Figure 60, Material utilised for all the components with CNC and SLM.

Figure 60 shows the material utilized for manufacturing the components of this study with two methods, CNC-machining and PBF-SLM. The bars are in stacked format to represent each process differently inside the total amount of material. The bars are in order of the component name, starting from the impeller produced with PBF, then the impeller complete with CNC-mill. Next is the impeller manufactured in the PBF, then is the manifold manufactured in CNC-lathe and CNC-mill, and finally, the gear lattice with PBF and the solid gear with CNC-mill. In green colour is the weight of the finished part in kilograms. There are three extra colours for the parts manufactured with the PBF-SLM method: PBF waste, EDM waste and CNC post-processing waste.

The most noticeable difference is that the lattice gear part weight is 0.090 kg, and the solid gear is 0.150 kg, but the waste generated with PBF for the lattice gear was higher than the solid gear manufactured with CNC. In total, both required almost the same amount of input material. The impeller CNC mill has more considerable waste than the PBF 30 µm and 50 µm. The final weight of the impeller component was 0.005 kg, which is different between the CNC and the PBF. The manifold manufactured with PBF 30 µm layer height had less material waste than the CNC-lathe and mill. The PBF-manufactured manifold was 0.010 kg heavier than the CNC-manufactured impeller. The reason for this could be the difference in material density. The PBF used SS316 L with a density of 8000 kg/m^3, and the CNC utilized a hexagonal

bar 11SMn30+C with a density of 7800 kg/m^3. The EDM waste was small for separating the build plate from the components in all cases.

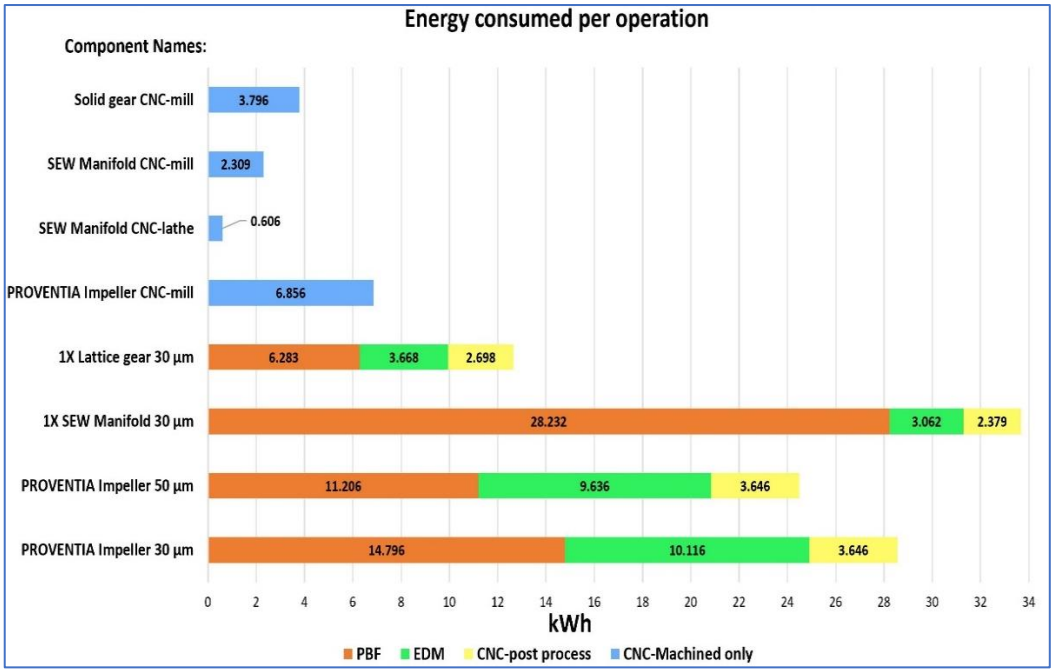

Figure 61, Total energy consumption per component manufactured with CNC and SLM.

Figure 61 shows the total energy consumed during the manufacturing phase of the components achieved in this study. In orange colour is PBF, referring to the SLM process. In green is the EDM, and in yellow is the CNC post-processing of the parts. These three processes were completed chronologically in that order. The bar chart is stacked to show the total energy during those three processes. In blue are represented the bars with CNC-machining only, with lathe and mill machine for the same components. The manifold has the highest energy consumption during printing with PBF compared to the CNC-lathe and the CNC-mill. This component manufactured with the CNC-lathe has a very small consumption of 0.606 kWh, and the second lowest energy is the CNC-mill with 2.309 kWh. The impeller made with a 50 µm layer height has lower energy consumption than the 30 µm layer height during the SLM process and EDM process. However, the impeller manufactured with a CNC-mill has 4.354 kWh less energy utilized for the manufacturing in comparison with the 50 µm layer PBF. The solid gear manufactured in the CNC-mill consumed 3.06 kWh less than the lattice gear in PBF only.

5 Discussion

In this study, the solid gear manufactured in the CNC- mill has less waste than the lattice gear manufactured with PBF SLM. However, if the solid gear is manufactured in the PBF SLM, it could have consumed more material and energy than the lattice pattern gear. Moreover, the tiny complex geometry makes manufacturing a lattice pattern gear on the CNC-machine is not possible.

From the energy measurement data of all the builds, it was seen that 40 % of the energy consumption of a single laser PBF machine came from the laser. In contrast, 60 % came from other machine components when the lasers were not in action. Therefore, a multi-laser machine may be more energy efficient for larger builds prints.

All the components were cut off from the build plate with EDM wire cutting, which had high energy consumption. On the other hand, if the detachment of the part was cut with a band saw machine, it might have consumed less energy, but also it could have wasted more material due to the thickness of the saw. Nevertheless, utilizing a band saw machine is also required to make CAD design changes in the components, adding more material to the bottom of the part. Ravisankar et. al. (2021) studied the operations of the SLM machine, founding that the coater motions, diode, and fibre laser activities account for minute-by-minute peaks in operating power usage. Therefore, adding extra material means more printing layers, more powder used, and more time the laser from the SLM machine is turned on, hence more electricity consumed.

Another important discovery was that one manufactured manifold with PBF consumed 33.672 kWh to become a fully functional part. That energy came from the SLM 3D printing, EDM builds plate cutting and the CNC post-processing machining. The CNC post-processing energy was very close to the energy consumed to manufacture the manifold completely just in the CNC-mill. Since the CNC-mill post-processing was 2.3790 kWh, and the CNC-mill was 2.309 kWh. The rest of the energy was to generate the whole structure from powder melted by the laser, consuming 28.232 kWh. Furthermore, this is an example of how the geometry shape for PBF does affect the final energy input.

Jiang et al. (2019) have performed an LCA comparison study between laser-engineered net shaping (LENS) and CNC-machining for gear manufacturing. In the LCA study, it was utilized as LCI inventory and as an energy input for the gear manufacturing 0.061 kWh with CNC-mill machine and 0.776 kWh with AM LENS method. Those energy consumption values are similar results to this thesis work, where AM consumed more energy than CNC. Adding on, Javaid et al. (2021) have arrived at the same conclusion that more waste can be produced by CM processes than by AM. One of the reasons

for that conclusion is that when utilizing a PBF machine, the majority of unused powder is reused in the next prints after it is sieved.

Deboer et al. (2021) performed an LCA comparison from AM and CM. In some portion of their study, the components were manufactured with a CNC-machine and PBF. They manufactured a double cardan joint H-yoke that has a complex geometry. The CNC-machined part was milled from a solid billet of 12.7 kg producing a waste of 10.63 kg. The different stages studied for this LCA were raw material forming, manufacturing phase, use and disposal phase. It was found that the life cycle of the component manufactured with CNC consumed more energy than those manufactured with PBF. Arguably, in their input data for the energy consumed during the manufacturing phase, CNC-machining had 11.802 kWh, while PBF had 222.15 kWh for the same component. Therefore, PBF had higher energy consumption during manufacturing than CNC. Thus, Deboer et al. (2021) energy values during the manufacturing phase match with this master thesis results. This highlights the fact that most often, PBF uses more energy during the manufacture (gate-to-gate), but when extended to a full LCA (cradle-to-grave), it may go in the other direction.

Liao & Cooper (2021) emphasise the importance of evaluating the actual literature on AM environmental impact carefully. Since some studies often do not consider in their calculations the post-processing from the PBF 3D printed parts. Thus, this can lead to unreliable information; for example, if the high energy consumption of EDM and the material waste from CNC-machining are neglected.

Faludi et al. (2017) studied the environmental impacts of the SLM machine by manufacturing an impeller on a SLM PBF with aluminium powder. That impeller is shown in figure 16 in this thesis. The SLM machine utilized was a Renishaw AM250 containing a 200 Watts laser. The study of Faludi et al. (2017) estimated that 208 cubic decimeters or 0.371 kg of argon gas was utilized per build operation. However, it is not stated in the study the measurement technique for the argon gas or which exact build operation. Faludi et al. (2017) further stated that the Renishaw AM250 utilized did not need a constant feed of argon gas during the printing operations and that the measurement of the argon gas had an uncertainty value of ±30 %. Considering the ±30 % of 0.371 kg, the argon gas measurement resembles the values found for the impeller 50 µm and the lattice pattern gear 30 µm in this thesis study. Furthermore, it is essential to notice that the Renishaw AM250 has a vacuum-sealed chamber that enables a lower argon gas consumption. (Engineering.com, 2022)

Finally, it is significant to remark that argon gas also contains primary embodied energy, as mentioned in chapter 2.3.1. Therefore, it is of paramount importance to state clearly how the argon gas is measured and for which exact build when performing an inventory for an LCA.

5.1 Conclusions

The most significant finding was that the CNC operation consumed less energy than PBF for all the studied components. The difference in energy consumption between the CNC-lathe manifold and the PBF manifold was over 50-fold. The energy consumption from the impeller 50 µm manufactured in PBF was 3.5 times greater than the impeller manufactured with CNC-mill. The lattice gear manufactured with PBF consumed 3.3 times more energy than the solid gear manufactured in the CNC-mill. In the PBF process, incrementing the layer thickness from 30 µm to 50 µm has reduced the waste material, argon gas and energy consumption by 16 %, 10 % and 10 %, respectively. The SLM process had surprisingly high material waste from the powder filters and sieving. The impeller component manufactured with the CNC-mill machine produced 62 % more material waste than the 50 µm layer 3D printed in the SLM. The lattice gear manufactured with SLM was 40 % lighter than the solid gear in the CNC-mill machine. However, the lattice gear generated in this study had 69 % more material waste than the solid gear, but in total, both of the components required almost the same amount of material to be manufactured.

Regarding sustainability, PBF is best suited for fabricating small, complex components that need extensive machining but less lasering. The lattice gear in this study is the best example of such a case, and the impeller also implies this. On the other hand, manufacturing the bulky manifold with PBF made little sense in terms of sustainability.

In closing, the geometry of the component will determine which process consumes less material and energy. Also, the components produced in PBF can be made lighter, as was shown with the lattice gear. Thus, the environmental benefits from PBF will be seen during the utilization phase of lightweight components when utilized in transport applications.

Research questions

The research questions have been answered successfully, for how much argon gas, metal powder and electricity were required for the PBF and how much feedstock material and electricity were required for the CNC-machining. For the other questions, the answer is the following:

- Which method is most suitable to manufacture with the least consumption of input materials?

The energy consumption from PBF was high, and that might not outweigh the lower material waste of CNC, and in some operations, PBF also had high material waste. Therefore, to have low consumption of inputs, it is necessary

to investigate the geometry of the component and functionality of the component case by case.

- What are the most relevant inputs flows for LCI of these manufacturing?

For the PBF, the most important input flows are the amount of material utilized, the amount of argon utilized as well with the energy consumption of the SLM machine. For CNC-machining, the most important input is to be exact and reliable in the measurement of the energy during manufacturing, as well as the amount of material utilized.

Implication & limitations of the thesis

Some practical implications of this study were that assumptions were made to obtain critical results. For example, for the warmup of the CNC-machines, the energy was divided by the possible number of parts that could be manufactured in one working day. There were no limitations when performing this study. The limitations pre-set in chapter 1.3 in the research strategy and scope chapter were the boundaries for the goal. The objectives of this thesis were accomplished without any difficulty.

Suggestions for further research

- Measurements of energy and material waste from cutting the components off the build plate with a band saw machine instead of EDM.
- The difference in consumption while printing the same component in a PBF-SLM machine with multiple lasers and higher productivity.
- Proper measurement of the embodied energy for powder production, gas atomization and argon gas production.
- Topology optimization of the parts to minimize material and energy usage in PBF.

Also, an LCA should be conducted in the future to determine which method has lower environmental impacts, as PBF tended to require less raw material but consumed more energy than CNC. This could reveal which method is more impactful in terms of total environmental impact. The data provided in this thesis will help to arrive at those conclusions in a later LCA that will be performed in the GREEF project.

References

Aalto University. (2022), “Green Factory - towards carbon neutral production (GREEF)”, available at: https://www.aalto.fi/en/department-of-mechanical-engineering/green-factory-towards-carbon-neutral-production-greef (accessed 3 November 2022).

ABB. (2013), “B23_212_100 Energy meter Manual, User. Product details.” available at: https://new.abb.com/products/2CMA100166R1000/ycu-00152 (accessed 26 December 2022).

Aneke, M. and Wang, M. (2015), “Improving the Energy Efficiency of Cryogenic Air Separation Units (ASU) through Compressor Waste Heat Recovery using Direct Binary Heat Engine Cycle”, pp. 2375–2380, doi: 10.1016/B978-0-444-63576-1.50090-X.

Ashby, M., Miller, A., Rutter, F., Seymour, C., Wegst, U. and Ashby, by. (2021), “Granta EduPack for Eco Design-A White Paper”, available at: https://www.ansys.com/content/dam/amp/2021/august/webpage-requests/education-resources-dam-upload-batch-3/eco-design-white-paper-PAPECOEN21.pdf (accessed 4 December 2022).

Bigot, S., Valentinčič, J., Blatnik, O. and Junkar, M. (2006), “Micro EDM parameters optimisation”, *4M 2006 - Second International Conference on Multi-Material Micro Manufacture*, Elsevier, pp. 195–198, doi: 10.1016/B978-008045263-0/50045-3.

Böckin, D. and Tillman, A.M. (2019), “Environmental assessment of additive manufacturing in the automotive industry”, *Journal of Cleaner Production*, Elsevier Ltd, Vol. 226, pp. 977–987, doi: 10.1016/j.jclepro.2019.04.086.

Boudreaux, K.A. (2022), “The parts of the periodic table”, *Angelo.Edu*, available at: https://www.angelo.edu/faculty/kboudrea/periodic/structure_mass.htm (accessed 13 December 2022).

Brillinger, M., Wuwer, M., Abdul Hadi, M. and Haas, F. (2021), “Energy prediction for CNC machining with machine learning”, *CIRP Journal of Manufacturing Science and Technology*, Vol. 35, pp. 715–723, doi: 10.1016/j.cirpj.2021.07.014.

Chandel, R.S., Kumar, R. and Kapoor, J. (2021), “Sustainability aspects of machining operations: A summary of concepts”, *Materials Today: Proceedings*, Elsevier Ltd, Vol. 50, pp. 716–727, doi: 10.1016/j.matpr.2021.04.624.

Crawford, R.H., Bontinck, P.A., Stephan, A., Wiedmann, T. and Yu, M. (2018), “Hybrid life cycle inventory methods – A review”, *Journal of Cleaner Production*, Elsevier Ltd, Vol. 172, pp. 1273–1288, doi: 10.1016/j.jclepro.2017.10.176.

Deboer, B., Nguyen, N., Diba, F. and Hosseini, A. (2021), “Additive, subtractive, and formative manufacturing of metal components: a life cycle assessment comparison”, *2021*, doi: 10.1007/s00170-021-07173-5/Published.

Diegel, O., Nordin, A. and Motte, D. (2019a), “Introduction to Additive Manufacturing”, pp. 1–17, doi: 10.1007/978-981-13-8281-9_1.

Diegel, O., Nordin, A. and Motte, D. (2019b), “Springer Series in Advanced Manufacturing A Practical Guide to Design for Additive Manufacturing”, doi: https://doi.org/10.1007/978-981-13-8281-9.

Dudley. (2012), “Handbook of Practical Gear Design and Manufacture”, Second Edition., ISBN-13: 978-1-4398-6602-3 (eBook - PDF).

Duque Ciceri, et al. (2010), “From Product End-of-Life Sustainable Considerations to Design Management”, *Springer*, pp. 152–159, doi: 10.1007/978-3-642-16358-6_20.

Engineering.com. (2022), “The Renishaw AM250 Additive Manufacturing System” Available at: https://www.engineering.com/story/the-renishaw-am250-additive-manufacturing-system (Accessed: December 23, 2022).

Faludi, J., Baumers, M., Maskery, I. and Hague, R. (2017), “Environmental Impacts of Selective Laser Melting: Do Printer, Powder, Or Power Dominate?”, *Journal of Industrial Ecology*, Blackwell Publishing, Vol. 21, pp. S144–S156, doi: 10.1111/jiec.12528.

Faludi, J., Bayley, C., Bhogal, S. and Iribarne, M. (2015), “Comparing environmental impacts of additive manufacturing vs traditional machining via life-cycle assessment”, *Rapid Prototyping Journal*, Emerald Group Publishing Ltd., Vol. 21 No. 1, pp. 14–33, doi: 10.1108/RPJ-07-2013-0067.

Finland Ministry of Environment, M. of. (2022), “Ministry of Environment Finland, Finland´s national climate change policy”, available at: https://ym.fi/en/finland-s-national-climate-change-policy (accessed 12 June 2022).

Fredriksson, C. (2019), “Sustainability of metal powder additive manufacturing”, *Procedia Manufacturing*, Elsevier B.V., Vol. 33, pp. 139–144, doi: 10.1016/j.promfg.2019.04.018.

GaBI software. (2011), “Introduction to LCA and modelling using GaBi. Paper clip tutorial. Part 1”, Stuttgart, 3 November, available at: www.pe-international.com (accessed 12 September 2022).

Gas Encyclopaedia Air Liquide. (2022), “Argon Physical Properties”, *Airliquide.Com*, available at: https://encyclopedia.airliquide.com/argon#properties (accessed 13 December 2022).

Al Geddawy, T. and ElMaraghy, H. (2016), “Design for energy sustainability in manufacturing systems”, *CIRP Annals*, Vol. 65 No. 1, pp. 409–412, doi: 10.1016/j.cirp.2016.04.023.

Gewinde Normen. (2022), “International Thread Standards”, 1 December, available at: https://www.gewinde-normen.de/en/whitworth-pipe-thread.html (accessed 30 November 2022).

GF Machining Solutions. (2022), “Mikron MILL E 500/700 U”, *Website*, available at: https://www.gfms.com/en-gb/machines/milling/5-axis/mikron-mill-e-500-700-u.html (accessed 12 December 2022).

Gibson, I., Rosen, D., Stucker, B. and Khorasani, M. (2021), “Powder Bed Fusion”, *Additive Manufacturing Technologies*, Springer International Publishing, Cham, pp. 125–170, doi: 10.1007/978-3-030-56127-7_5.

Global Carbon Project, G. (2022), “The World Counts, Tons of CO2 emitted into the atmosphere globally this year”, available at: https://www.theworldcounts.com/challenges/climate-change/global-warming/global-co2-emissions (accessed 3 December 2022).

Grahl B &. Klöpffer, W. (2014). (2014), “Life Cycle Assessment (LCA): A Guide to Best Practice. Weinheim: Wiley-VCH Verlag GmbH & Co. KgaA. ISBN: 978-3-527-65565-6.”

Hajnys, J., Pagac, M., Mesicek, J., Petru, J. and Spalek, F. (2020), “Research of 316L Metallic Powder for Use in SLM 3D Printing”, *Advances in Materials Science*, Walter de Gruyter GmbH, Vol. 20 No. 1, pp. 5–15, doi: 10.2478/adms-2020-0001.

Höganäs. (2022), “Metal powder Stainless steel 316L”, available at: https://www.hoganas.com/en/powder-technologies/products/hot-polymer-filtration-powders/316l/ (accessed 13 December 2022).

Huang, R., Riddle, M., Graziano, D., Warren, J., Das, S., Nimbalkar, S., Cresko, J., *et al.* (2016), “Energy and emissions saving potential of additive manufacturing: the case of lightweight aircraft components”, *Journal of Cleaner Production*, Elsevier Ltd, Vol. 135, pp. 1559–1570, doi: 10.1016/j.jclepro.2015.04.109.

Huppes, G. and Suh, S. (2005), “Methods for life cycle inventory of a product”, *Journal of Cleaner Production*, Elsevier Ltd, Vol. 13 No. 7, pp. 687–697, doi: 10.1016/j.jclepro.2003.04.001.

Hyatt, G., Piber, M., Chaphalkar, N., Kleinhenz, O. and Mori, M. (2014), “A Review of New Strategies for Gear Production”, *Procedia CIRP*, Vol. 14, pp. 72–76, doi: 10.1016/j.procir.2014.03.034.

Islam, S., Ponnambalam, S.G. and Lam, H.L. (2016), “Review on life cycle inventory: methods, examples and applications”, *Journal of Cleaner Production*, Elsevier Ltd, Vol. 136, pp. 266–278, doi: 10.1016/j.jclepro.2016.05.144.

ISO 14040:2006. (2006), “Environmental Management. Life cycle assessment principles and framework (ISO 14040:2006)”.

Javaid, M., Haleem, A., Singh, R.P., Suman, R. and Rab, S. (2021), “Role of additive manufacturing applications towards environmental sustainability”, *Advanced Industrial and Engineering Polymer Research*, Vol. 4, KeAi Communications Co., pp. 312–322, doi: 10.1016/j.aiepr.2021.07.005.

Jiang, Q., Liu, Z., Li, T., Cong, W., and Zhang, H.C. (2019), “Emergy-based life-cycle assessment (Em-LCA) for sustainability assessment: a case study of laser additive manufacturing versus CNC machining”, *International Journal of Advanced Manufacturing Technology*, Springer London, Vol. 102 No. 9–12, pp. 4109–4120, doi: 10.1007/s00170-019-03486-8.

Joni Reijonen. (2022), “Interview-discussion with Research Scientist from VTT Oy. about Powder manufacturing and PBF.”, Espoo, Finland, 12 December.

Liao, J., and Cooper, D.R. (2021), “The environmental impacts of metal powder bed additive manufacturing”, *Journal of Manufacturing Science and Engineering, Transactions of the ASME*, American Society of Mechanical Engineers (ASME), Vol. 143 No. 3, doi: 10.1115/1.4048435.

Liu, Z.Y., Li, C., Fang, X.Y. and Guo, Y.B. (2018), “Energy Consumption in Additive Manufacturing of Metal Parts”, Elsevier B.V., Vol. 26, pp. 834–845, doi: 10.1016/j.promfg.2018.07.104.

Malek-Khatabi, A., Faraji Rad, Z., Rad-Malekshahi, M. and Akbarijavar, H. (2023), “Development of dissolvable microneedle patches by CNC machining and micromolding for drug delivery”, *Materials Letters*, Elsevier B.V., Vol. 330, doi: 10.1016/j.matlet.2022.133328.

Marashi, H., Sarhan, A.A.D., Maher, I. and Sayuti, M. (2017), “1.7 Techniques to Improve EDM Capabilities: A Review”, *Comprehensive Materials Finishing*, Elsevier, pp. 171–202, doi: 10.1016/B978-0-12-803581-8.09153-0.

Md Imran Hossen. (2022), “Turbo compressor wheel Design in SolidWorks 2021”, *White GrabCAD Logo © 2022 Stratasys Inc.*, 11 November, available at: https://grabcad.com/library/turbo-compressor-wheel-8 (accessed 8 December 2022).

Moghimian, P., Poirié, T., Habibnejad-Korayem, M., Zavala, J.A., Kroeger, J., Marion, F. and Larouche, F. (2021), “Metal powders in additive manufacturing: A review on reusability and recyclability of common titanium, nickel and aluminium alloys”, *Additive Manufacturing*, Elsevier B.V., Vol. 43, doi: 10.1016/j.addma.2021.102017.

NASA Earth Observatory, Nasa. gov. (2022), “NASA Earth Observatory, World of Changes: Global Temperatures”, available at: https://earthobservatory.nasa.gov/world-of-change/global-temperatures (accessed 17 August 2022).

Nippon Gases. (2020), “Argon for additive manufacturing”, *Copyright © 2020 Nippon Gases*, available at: https://nippongases.com/fr-en/gases/ar-for-am (accessed 5 December 2022).

Ochs, D., Wehnert, K.K., Hartmann, J., Schiffler, A. and Schmitt, J. (2021), “Sustainable Aspects of a Metal Printing Process Chain with Laser Powder Bed Fusion (LPBF)”, *Procedia CIRP*, Elsevier B.V., Vol. 98, pp. 613–618, doi: 10.1016/j.procir.2021.01.163.

Papetti, A., Menghi, R., di Domizio, G., Germani, M. and Marconi, M. (2019), “Resources value mapping: A method to assess the resource efficiency of manufacturing systems”, *Applied Energy*, Vol. 249, pp. 326–342, doi: 10.1016/j.apenergy.2019.04.158.

Peng, T., Kellens, K., Tang, R., Chen, C. and Chen, G. (2018), “Sustainability of additive manufacturing: An overview on its energy demand and environmental impact”, *Additive Manufacturing*, Elsevier, Vol. 21, pp. 694–704, doi: 10.1016/J.ADDMA.2018.04.022.

Peng, T., Wang, Y., Zhu, Y., Yang, Y., Yang, Y. and Tang, R. (2020), “Life cycle assessment of selective-laser-melting-produced hydraulic valve body with integrated design and manufacturing optimization: A cradle-to-gate study”, *Additive Manufacturing*, Elsevier B.V., Vol. 36, doi: 10.1016/j.addma.2020.101530.

Pessoa, R., Profile, S., Hoyer, Y.D. and Maciel, H.S. (2013), “Argon properties, production and recent applications”, ISBN:978-1-62618-243-1(eBook).

Pramanik, Alokesh. and Basak, A. Kumar. (2015), “Stainless steel: microstructure, mechanical properties and methods of application”, in Pramanik A. and K. Basak (Eds.), Vol. Chapter 2, Nova Science Publishers, ISBN 9781634820806.

Proventia Oy. (2022), “Proventia.com”, 3 November, available at: https://www.proventia.com/ (accessed 3 November 2022).

Ramadani, R., Belsak, A., Kegl, M., Predan, J. and Pehan, S. (2018), “Topology optimization-based design of lightweight and low vibration gear bodies”, *International Journal of Simulation Modelling*, Vienna University of Technology, Vol. 17 No. 1, pp. 92–104, doi: 10.2507/IJSIMM17(1)419.

Rashid, A., and Jahan, M.P. (2021), “Microfabrication by electrical discharge machining-based hybrid processes”, *Micro Electro-Fabrication*, Elsevier, pp. 33–62, doi: 10.1016/B978-0-12-820049-0.00008-6.

Ravisankar, B., Jaeger, E., Meißner, M., Wirtz, A., Wiederkehr, P. and Rehtanz, C. (2021), “Investigation of electrical power consumption of an additive process chain and empirical modelling as feature selection for

machine learning algorithms", *Procedia CIRP*, Vol. 99, pp. 358–363, doi: 10.1016/j.procir.2021.03.103.

Reinecke, H., Müller, C. and Karazi, S.M. (2016), "Micromachining", *Reference Module in Materials Science and Materials Engineering*, Elsevier, doi: 10.1016/B978-0-12-803581-8.00531-2.

Reuter, M., Peltomäki, M., Horn, S. and Nuppumäki, E. (2020), "HSC-Sim LCA Metso Outotec reserves the right to modify these specifications at any time without prior notice", available at: https://www.mogroup.com/globalassets/portfolio/hsc-chemistry/49-sim-lca.pdf (accessed 26 December 2022).

Salmi, M. (2021), "Additive Manufacturing Processes in Medical Applications", *Materials*, Vol. 14 No. 1, p. 191, doi: 10.3390/ma14010191.

Sandvik. (2022), "Invomilling manufacturing of spur gears", available at: https://www.sandvik.coromant.com/en-gb/tools/digital-machining/coroplus-tool-path/invomilling (accessed 1 December 2022).

Seppänen, R. and Jansson, N. (2006), "MAOLs tabeller: matematik, fysik, kemi", *Finna.Fi*, Vol. 8.

SEW Eurodrive.fi. (2022), "SEW Eurodrive", *Website Finland*, 3 November, available at: https://www.sew-eurodrive.fi/koti.html (accessed 3 November 2022).

Shelly EM. (2022), "Energy meter 120A Clamp from Shelly EM", *Https://Www.Shelly.Cloud/En/Products/Shop/Em-120a*, available at: https://www.shelly.cloud/en/products/shop/em-120a (accessed 13 December 2022).

Van Sice, C. and Faludi, J. (2021), "Comparing environmental impacts of metal additive manufacturing to conventional manufacturing", *Proceedings of the Design Society*, Cambridge University Press, Vol. 1, pp. 671–680, doi: 10.1017/pds.2021.67.

SLM solutions. (2022), "Selective Laser Melting System Accurate, compact and highly performant options for fast results For production of highly complex components in research and development", available at: https://pdf.directindustry.com/pdf/slm-solutions/slm-125-hl/114591-626986-_4.html (accessed 12 December 2022).

Song, X., Zhai, W., Huang, R., Fu, J., Fu, M.W. and Li, F. (2022), "Metal-Based 3D-Printed Micro Parts & Structures", *Encyclopaedia of Materials: Metals and Alloys*, Elsevier, pp. 448–461, doi: 10.1016/B978-0-12-819726-4.00009-0.

Soundararajan, B., Sofia, D., Barletta, D. and Poletto, M. (2021), "Review on modelling techniques for powder bed fusion processes based on physical principles", *Additive Manufacturing*, Vol. 47, p. 102336, doi: 10.1016/j.addma.2021.102336.

Statista. (2022), “Finland: Share of economic sectors in the gross domestic product (GDP) from 2011 to 2021”, available at: Finland: Share of economic sectors in the gross domestic product (GDP) from 2011 to 2021 (accessed 30 November 2022).

Steel Navigator. (2022), “11SMn30 steel hexagonal bar Properties”, available at: https://steelnavigator.ovako.com/steel-grades/green-cut/ (accessed 13 December 2022).

Steuer, P., Rebschläger, A., Weber, O. and Bähre, D. (2014), “The Heat-affected Zone in EDM and its Influence on a Following PECM Process”, *Procedia CIRP*, Vol. 13, pp. 276–281, doi: 10.1016/j.procir.2014.04.047.

Teknologiateollisuus. (2020), “TEKNOLOGIATEOLLISUUS, Low-carbon road map for technology industry 2035”, available at: https://teknologiateollisuus.fi/sites/default/files/inline-files/Teknologiateollisuudenva%CC%88ha%CC%88hiilitiekartta-tiivistelm%C3%A4_2020-06-08_FINAL.pdf (accessed 25 October 2022).

Thyssenkrupp Materials (UK) Ltd. (2022), “Stainless Steel 316L,1.4404 Material Data Sheet”, available at: https://d2z035mdb530wx.cloudfront.net/_legacy/UCPthyssenkruppBAMXUK/assets.files/material-data-sheets/stainless-steel/stainless-steel-1.4404-316l.pdf (accessed 13 December 2022).

Toolbox Finland. (2021), “Toolbox Finland Climate Solutions From Finland, ‘Ministry for Foreign Affairs of Finland’”, available at: https://toolbox.finland.fi/wp-content/uploads/sites/2/2022/01/finfo_climate_en_auk.pdf (accessed 25 October 2022).

Trading Economics. (2022), “Finland Manufacturing Production”, available at: https://tradingeconomics.com/finland/manufacturing-production (accessed 25 October 2022).

UCAR. (2022), “What’s in the Air?”, *UCAR Canter for Science and Education.*, available at: https://scied.ucar.edu/learning-zone/air-quality/whats-in-the-air (accessed 5 December 2022).

UNFCCC. (2015), “United Nations For Climate Change, The Paris Agreement”, available at: https://unfccc.int/process-and-meetings/the-paris-agreement/the-paris-agreement (accessed 25 October 2022).

University of Oulu. (2022), “Green Factory Towards Carbon Neutral Production”, *Https://Www.Oulu.Fi/En/Projects/Green-Factory-towards-Carbon-Neutral-Production-0*, 3 November, available at: https://www.oulu.fi/en/projects/green-factory-towards-carbon-neutral-production-0 (accessed 3 November 2022).

Woikoski Oy. (2022), “Argon Ar 50 L 200 bar DIN 10 RPV”, *Woikoski.fi*, available at: https://woikoskistore.woikoski.fi/t200060-argon-ar-50-l-200-bar-din-10-rpv.html (accessed 13 December 2022).

World Economic Forum.org. (2016), “World Economic Forum Fourth Industrial Revolution: what it means, how to respond”, available at: https://www.weforum.org/agenda/2016/01/the-fourth-industrial-revolution-what-it-means-and-how-to-respond/#:~:text=When%20compared%20with%20previous%20industrial%20revolutions%2C%20the%20Fourth%20is%20evolving%20at%20an%20exponential%20rather%20than%20a%20 (accessed 25 October 2022).

Yi, L., Ehmsen, S., Glatt, M. and Aurich, J.C. (2020), “A case study on the part optimization using eco-design for additive manufacturing based on energy performance assessment”, *Procedia CIRP*, Elsevier B.V., Vol. 96, pp. 91–96, doi: 10.1016/j.procir.2021.01.058.

Zhang, P., Liu, Z., Du, J., Su, G., Zhang, J. and Xu, C. (2020), “On machinability and surface integrity in subsequent machining of additively-manufactured thick coatings: A review”, *Journal of Manufacturing Processes*, Elsevier Ltd, Vol. 53, pp. 123–143, doi: 10.1016/j.jmapro.2020.02.013.